Universitetet i Stavanger

FACULTY OF SCIENCE AND TECHNOLOGY

MASTER'S THESIS

Study program/Specialization: **Offshore Technology/Marine and Subsea Technology**	Spring semester, 2018 **Open**
Author: **Antonius Lasut**	…… (signature of author)
Faculty Supervisor: **Dr. Charlotte Obhrai**	
Title of master's thesis: **Occurrence of Wind-Wave Misalignment using FINO and OBLEX data**	
Credits (ECTS): **30**	
Keywords: FINO 1, FINO 3, OBLEX, wind-wave misalignment, swell wave, turbulence intensity, wind profile, offshore wind turbine	Number of pages: 77 +enclosure : - Stavanger, 15th June 2018

Abstract

Wind-wave interaction has been an important aspect of environmental conditions to be considered for offshore wind turbine performance, especially in deeper water at stable atmospheric conditions such as North Sea. It is generally understood that ocean waves are thought to be influenced by the surface wind that transfers momentum from the atmosphere to the waves. However, recent observations have suggested that when swell persist with faster propagation than the surface wind, momentum from waves can also transfer to the atmosphere.

It is not uncommon for the wind and waves to be misaligned, and this situation can result in interesting features that may have an impact on the power production, turbulence generation, and fatigue damage to the wind turbine. In general, there are misalignments between the wind and waves at all wind speeds: small misalignments at large wind speeds and large misalignments at lower wind speeds. The largest misalignments are associated with stable atmospheric conditions (Bachynski et al., 2014). Furthermore, Bachynski et al. (2014) using observations from the North Sea suggest that misalignment of up to 30° is common, while misalignment larger than 60° occur less than 5% of the time.

In this thesis, MATLAB analysis of 11 years of data from FINO 1 and 8 years data from FINO 3 has been conducted to determine the frequency of occurrence of wind wave misalignment under swell and wind wave conditions. Waves are usually aligned with the wind. However, swell do not always correlate to the direction of the wind. In this study, the frequency of occurrences of wind-wave misalignment are studied and the effects of the aligned and misaligned wind-wave on distribution of wind speed have also been checked. Total misalignment and opposing misalignment for platforms FINO 1 and FINO 3 were observed higher in FINO 1. In the other hand, wind-wave misalignment under swell were found to occur less than the ones under wind wave.

Turbulence intensities in each site was analysed according to the classification of wind-wave misalignment and it was found that the turbulence intensity under opposing wind-wave was lower compared to the perpendicular and aligned conditions. Wind profile at FINO 1 was observed as well, taking into account the lower heights measurement at OBLEX campaign. A 1-month period between September and October 2015 was selected based on availability of data. Observation by plotting mean wind speed data from FINO 1 and OBLEX resulted in wind profiles as expected. However, an interesting point to see is that the mean wind speed at the lowest measurement 15 m LAT is higher than the wind speed at 20 m LAT which may well get an accelerated wind speed because of the position of sonic anemometer at 15 m height relative to the position of sonic anemometer at 20 m.

Acknowledgements

Firstly, I would like to express my sincere gratitude to my advisor Dr. Charlotte Obhrai for the continuous support of my thesis work, especially for her patience, motivation, and extensive knowledge. This work would not have been completed without her valuable mentoring in areas of coding and data interpretation. I really value her for her intelligence, ideas, and insight that have been inspired me in many ways. Her guidance helped me to understand the problems with more depth, and steered me to the right direction.

To Mr. Markus Kreklau for providing the access to the FINO data base, and especially the BMWi (Bundesministerium fuer Wirtschaft und Energie, Federal Ministry for Economic Affairs and Energy) and the PTJ (Projekttraeger Juelich, project executing organization) as the owner of FINO data base. Particularly for the meteorological and oceanographic data that were under supervision of Deutsches Windenergi Institut (DEWI) and The Federal Maritime and Hydrographic Agency of Germany (BSH), respectively.

To Martin Flügge from Christian Michelsen Research AS (CMR) that has provided with access to the OBLEX-F1 data base, and for his swift help regarding the information necessary to finish this study. All personnel and resources from University of Bergen (UoB) and CMR who had carried out this campaign. Particularly for NORCOWE, as the owner of the OBLEX-F1 data base.

To my parents, my sister and brothers who always support me during my studies, and to all my friends in Marine and Subsea Technology study programme, thank you for the lesson and cooperation.

Stavanger, June 14th 2016

Antonius Lasut

Table of Contents

List of Figures

List of Tables

Nomenclature

Symbols

K	von Karman constant
L	Monin-Obukhov length
Hs	Significant Wave Height
Tp	Peak Wave Period
z_0	Roughness Length
α	Power Law Exponent
A_c	Charnock Constant
σ_u	Standard Deviation of Wind Speed
χ_{10}	Wave Age
C_p	Phase Speed of Wave
E	Wave Energy
f_p	Wave Peak Frequency
X	Fetch
u	Wind Speed
u_0*	Wind Stress Velocity
g	Gravity Acceleration

Abbreviations

ABL	Atmospheric Boundary Layer
AWAC	Acoustic Wave and Current Meter
BSH	The Federal Maritime and Hydrographic Agency of Germany
DEWI	Deutsches Windenergi Institut
CFD	Computational Fluid Dynamics
EC	Environmental Conditions
DNV	Det Norske Veritas
EAZ	Egmond aan Zee
FAST	Fatigue, Aerodynamics, Structures, and Turbulence
FINO	Forschung In Nord und Ostsee
LAT	Lowest Astronomical Tide
LES	Large Eddy Simulations
MABL	Marine Atmospheric Boundary Layer
NESS	North European Storm Study
NNW	North-North-West
NORCOWE	The Norwegian Centre for Offshore Wind Energy
NW	North-West
OBLEX	Offshore Boundary Layer Experiment
PBL	Planetary Boundary Layer
SWL	Sea Water Level
SE	South-East
TI	Turbulence Intensity
USA	Ultrasonic Anemometer
WSW	West-South-West

1. Introduction

1.1 Background

Waves can have a significant influence on wind profiles and the performance of offshore wind turbines. This phenomenon and its effects have not been considered yet in the design and calculation phase, as well as when estimating the power production of wind turbine. Wind-wave misalignment is defined as the temporal difference between the wind direction and the mean wave direction of wind-generated waves (Kühn, 2001; Vledder, 2013). Situations where the wind and the waves are out of phase and misaligned to each other can result in interesting features that may have an impact to the power production, turbulence generation, and fatigue damage to the wind turbine. However, analysis of these concepts is a fairly young field, and much of the researches have been limited to environmental conditions (ECs) where wind and waves arrive from the same direction (Bachynski et al., 2014). It is not unusual for wind and waves to be misaligned, particularly in stable atmospheric conditions.

Model experiments show that waves influence wind field above them (Sullivan et al., 2008). The effect is notable up to the marine atmospheric boundary layer (MABL) and depends on the wave state and the direction of waves and wind. As a result, a wind turbine rotor is exposed to wind profiles and turbulent levels which are not predicted with the conventional assumption of logarithmic wind profile and low turbulence levels over a flat surface. Model simulations with a coupled setup further show that wave influenced wind affects the turbine performance, as well as the load and fatigue (Kalvig, 2014). A wide range of met-ocean conditions were investigated, and the extreme loads were found to occur at the maximum significant wave height and for high wind/wave misalignments (Barj et al., 2014). Therefore, it is important to assess the statistical significance of wind-wave misalignment using long-term measured offshore wind data.

1.2 Objective

This master thesis intends to investigate the occurrence of wind-wave misalignment cases using long term data measurement from the FINO 1 and FINO 3 platforms. The 10-minutes average wind speed, wind direction, wave height, wave period, and wave direction have been used to determine the prevalence of wind and wave misalignment, especially during the swell wave conditions (long period waves). Other objective includes analysing the wind profile and

turbulence intensity by introducing lower height measurement from the OBLEX-F1 (Offshore Boundary Layer Experiment at FINO 1) campaign by NORCOWE, with several new instruments added to investigate atmospheric surface and boundary layer.

Ultimately, the collected and analysed data regarding the occurrence of wind-wave misalignment can be used to validate and improve numerical models and tools in various application fronts such as weather forecasting, marine operations, power performance, and wind farm layout and accessibility.

1.3 Thesis structure

The structural outline of this thesis has been presented in Figure 1.1 below. Most of the steps was dependent to the previous milestone, since this study was a continuous work. In this study, a large number of data was processed, therefore comprehensive work was performed to avoid errors. The processed data were double-checked to ensure the validity.

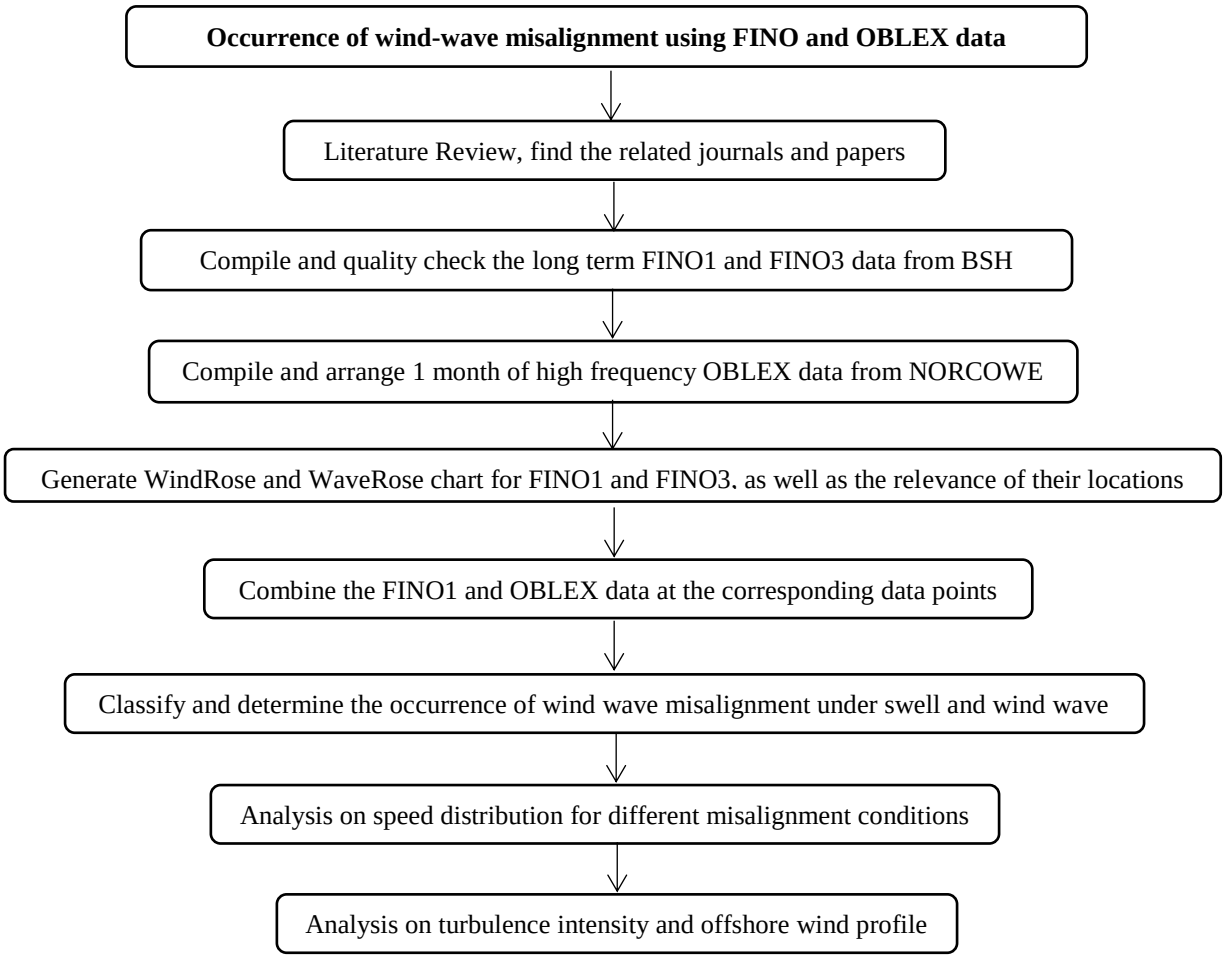

Figure 1.1 Thesis Structure.

2. Basic theory

2.1 Offshore wind energy

Onshore wind turbines have been the main infrastructure to capture wind energy for nearly the entire history of wind power. The conventional horizontal axis, three-blade wind turbines placed on open space such as farms, grassy plains or desert surfaces have been a reliable choice in terms of installation, structure stability, and cost. However, they do not produce energy constantly throughout the year due to low wind speed and reduced performance in the presence of physical obstacle such as hills or buildings. On the other hand, without physical restriction such as those on the land, offshore wind turbine can be built much bigger and taller, capturing higher wind speed, thus allowing for more power production.

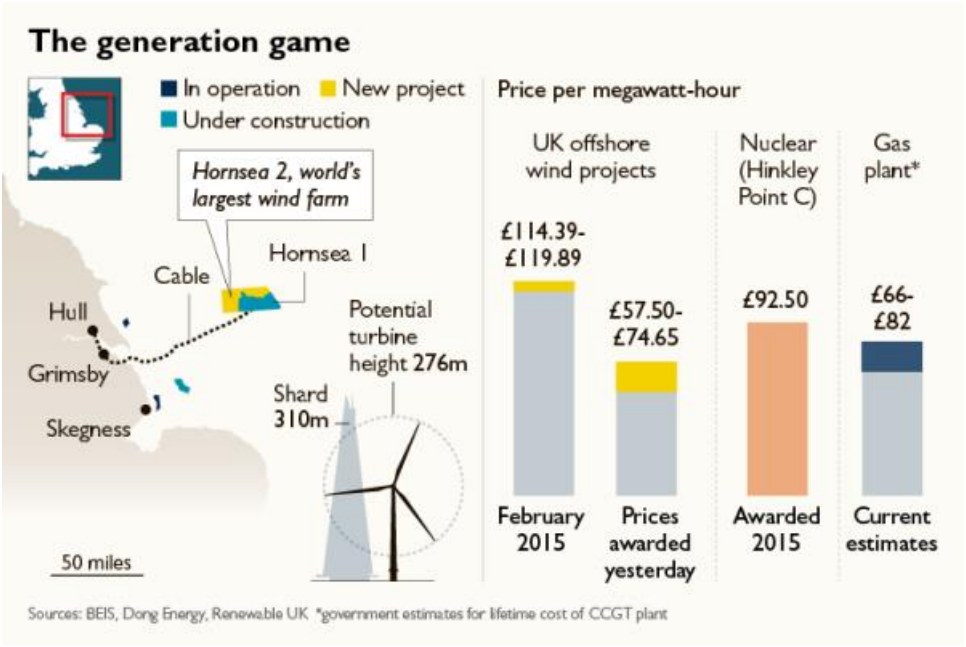

Figure 2.1. Schematic of Hornsea Projects offshore wind farm (Gosden, 2017).

Those advantages were considered as the driving force for the growing number of offshore wind turbine installations in the world, especially in Europe, where in 1991 Vindeby Offshore Wind Farm became the pioneer of offshore wind farm installation that contained 11 units wind turbine with total capacity 4.95 MW and hub height (height from SWL to the axis of wind turbine rotor) 35 m (EWEA, 2009). Meanwhile in 2020 and 2022, the ongoing Hornsea Project 1 and 2, the world biggest offshore wind farm projects will begin operation in North Sea off coast of UK which are claimed to be cheaper than gas and nuclear energy. (Gosden, 2017). The schematic of location, status and estimated price per megawatt-hour of the Hornsea projects is

shown at Figure 2.1 above. We can see that offshore wind energy is slowly becoming a serious competitive form of alternative energy. Therefore, research in terms of offshore environmental sea-state (i.e. wind-wave interaction, wind-wave misalignment) and marine operation is gaining more impetus for offshore wind turbine performance.

2.2 Planetary Boundary Layer

The planetary boundary layer (PBL) is the lowest part of the atmosphere which is directly influenced by the earth's surface. Therefore, much of the weather that is experienced is a result of PBL changes. Due to aerodynamic drag, a wind gradient is formed in the wind flow several hundred meters above the Earth's surface. Wind speed increases with increasing height above Earth's surface, starting from zero, because of the no-slip condition (Stull, 1988).

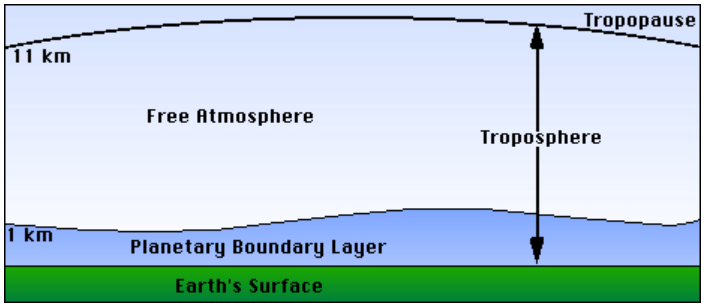

Figure 2.2. Planetary Boundary Layer (PBL) (shodor.org, accessed 2017).

At some point in the atmosphere, there is a zone where friction goes from significant to insignificant (Stull, 1988). The lower layer of air which is subjected to turbulent (frictional) processes is known as the planetary boundary layer (PBL). The remaining air in the troposphere is known as the free atmosphere as it is free of frictional influences.

Below is the comparison between the PBL and the free atmosphere characteristics.

Table 2.1 Comparison between PBL and Free Atmosphere.

Property	Planetary Boundary Layer	Free Atmosphere
Friction	Significant drag against earth's surface. High energy dissipation (due to friction)	Up to 10km above the ground
Turbulence	Continuous turbulence throughout layer	Less friction Low energy dissipation
Thickness	Between 100 and 3000 m, diurnal variation over land	Only near jet stream and convective clouds

Mixing	Rapid turbulent mixing in vertical and horizontal	Low mixing in vertical Mixing in horizontal
Wind Profile	High vertical wind shear	Low vertical wind shear

2.2.1 Atmospheric Boundary Layer

Atmospheric boundary layer (ABL) is another term to explain the layer where atmosphere is in contact with ground surface, land, or sea. The surface-air interaction is the trigger of the ABL formation and is occurring in two primary forms (Cushman-Roisin, 2014):

- Mechanical:
    - Arises from the friction exerted by wind against ground surface; causes wind shear and creates turbulence.
    - When ABL is said to be in neutral condition, we expect wind profile which characterized by friction velocity and roughness length, see Chapter 2.3.
- Thermal:
    - The origin is solar radiation. Sun light is electromagnetic radiation in the visible range, which is visually transparent in the atmosphere. Therefore, most of the solar radiation passes through atmosphere and reaches surface.
    - Most of the solar radiation is absorbed immediately below earth surface, which heats up and then radiates heat back. This radiation is emitted upward into the atmosphere, and while some portion escapes to space, much of it is retained in the atmosphere because of water vapor, carbon dioxide and other gases. This heat retention is called the *greenhouse effect.*

2.2.2 Marine Atmospheric Boundary Layer

Marine Atmospheric Boundary Layer (MABL) simply means atmospheric boundary layer which exist on the surface of the sea. MABL shows significant differences compared to the ABL over flat homogeneous ground. Wind speeds are higher and turbulence intensities are lower in the MABL compared to those in the onshore ABL. Advantages of wind conditions in offshore can also be seen by the lower vertical wind shear compared to onshore. This means that the wind speeds over the ocean are much more consistent.

Main differences of MABL and ABL are summarised below (Arya, 1988):

- Large differences in the energy balance of sea and land

- Heat Capacity

  Water has a higher heat capacity than land. It therefore needs more heat to raise the temperature of one gram of water by one degree than it does to raise the temperature of land.

- Non-stationary lower boundary of sea vs. stationary lower boundary of land
  - Ocean waves vs. flat homogeneous ground.

    On flat homogeneous ground, the boundary layer affects the wind profile in a smooth increment as seen in the left-side wind profile in Figure 2.3. Meanwhile, at sea, the lower boundary layer is not stationary due to wave, therefore the influence of shear stress on the surface of the sea will be either reinforcing or diminishing the wind speed at near surface. This phenomenon is illustrated by the central and the right wind profile shown in Figure 2.3.

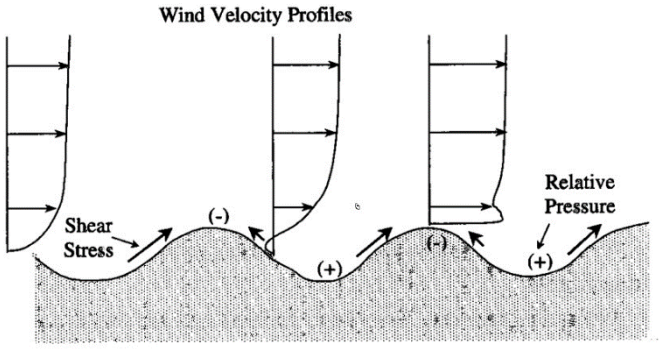

Figure 2.3. Non-stationary lower boundary.

- Surface roughness offshore is lower than onshore
  - The lower surface roughness offshore results in a very different vertical structure of the boundary layer, i.e. the depth of the surface layer can be as low as 30m.
- Relevant measurements over the ocean are sparse or non-existent.

For wind energy calculations, there are a lot of variables and aspects that needs to be considered which are often changing rapidly. Therefore, generally neutral stratification and a flat, smooth sea surface are routinely used as the assumptions in wind energy calculations (Kalvig, Gudmestad, et al., 2014).

Knowledge of the MABL is important in offshore industry in terms of (a) assessing wind resource (e.g. wind-wave misalignment) and defining design criteria for structural load (e.g. occurrence of extreme winds) in the planning phase, (b) defining weather windows favourable for marine operations during the construction phase (e.g. heavy lift operations), (c) measuring

actual flow conditions such as wind speed, turbulence intensity as well as accessibility for operation and maintenance in the operational phase.

2.2.3 Wind Boundary Layer

As shown in previously in Figure 2.2, the Planetary Boundary Layer is the layer closest to the earth surface and therefore the most relevant for wind turbine operation. This boundary layer is divided into Surface Layer and Ekman (transition) Layer, illustrated in Figure 2.4, which also shows the way in which the wind speed changes with height. This characteristic is called velocity shear and the shape of the curve is known as the wind shear profile (Martin, 2010). The design of wind turbines is engineered according to the characteristics of the Surface Layer since the height of most wind turbines are ranging from 50 m up to 200 m. However, in the MABL, the surface layer height can be as low as 30 m under stable atmospheric conditions (Emeis, 2014).

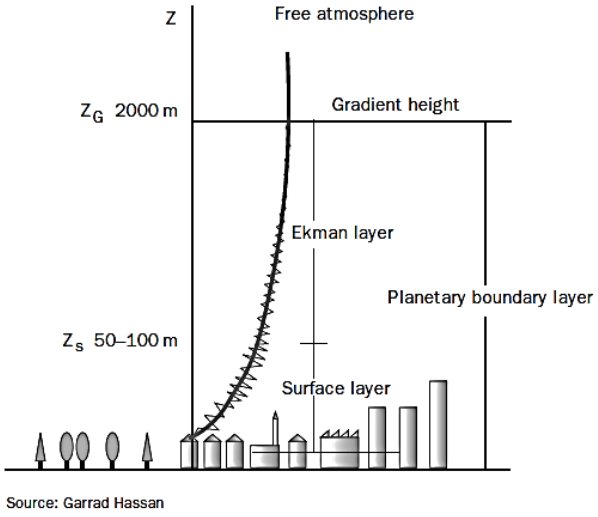

Figure 2.4 The atmospheric boundary layer shear profile (Hassan, 2018).

2.3 Wind profiles

The variations of the mean wind speed with height above the still water level is called wind profile. It is affected by several factors, such as roughness length, friction velocity, and atmospheric stability.

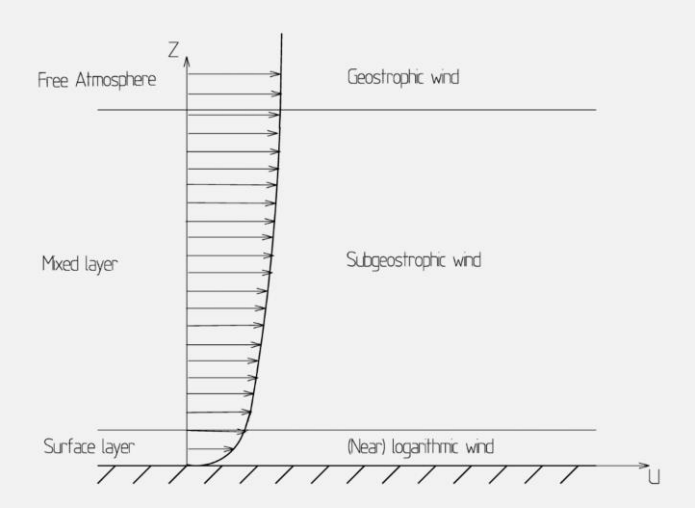

Figure 2.5. Typical wind profile in the boundary layer.

In a non-complex terrain and atmospheric conditions, wind speed profile may be represented by an idealised wind profile. There are three common wind profiles namely logarithmic wind profile, power law wind profile, and stability corrected wind profile.

2.3.1 Power law wind profile

In wind power assessments, the power law is often used as the simplified form when estimating the wind speed above the surface layer. However, there is height limit which is considered to produce reliable results, and also is accounted for lower heights above sea water level (SWL) up to 50 m (Peterson & Jr., 1978). Relationship between wind speeds at different heights with power law is calculated as below:

$$U(z) = U_{ref}\left(\frac{z}{z_{ref}}\right)^{\alpha} \tag{2.1}$$

Where,

$U(z)$ = wind speed at height z

U_{ref} = mean wind speed at z_{ref}

z_{ref} = reference height

z = target estimated height

α = power law exponent

The power law exponent is an empirically derived coefficient which value is depends on the stability of the atmosphere and surface roughness. For neutral stability conditions, α is 1/7 or 0.143, assuming constant sea surface roughness of 0.002 m.

2.3.2 Logarithmic wind profile

Logarithmic wind profile is a semi-empirical relationship of wind profile which is used for neutral atmospheric conditions within the lowest section of boundary layer. The logarithmic wind profile is considered a more reliable estimator of mean wind speed compared to power law wind profile in the lowest 10-20 m of the surface boundary layer (Cook, 1986). Generally, reliable result can be obtained up to 100 m above Sea Water Level (SWL) depending on the height of the surface layer. The relationship between wind speeds at different heights with logarithmic law is given as below:

$$U(z) = \frac{U_*}{k} \ln\left(\frac{z}{z_0}\right) \tag{2.2}$$

Where,

U_* = friction velocity

k = Von Karman constant (0.4)

z_0 = roughness length

z = target estimated height

If the wind speeds at certain height is known, then equation above can be re-written as:

$$U(z) = U_{ref} \frac{\ln\left(\frac{z}{z_0}\right)}{\ln\left(\frac{z_{ref}}{z_0}\right)} \tag{2.3}$$

2.3.3 Stability corrections wind profile

The validity of wind profile estimators is affected by the atmospheric stability. Therefore, we need to adjust the estimator formula to achieve the appropriate value under different stability conditions. Stability corrections wind profile are made from the logarithmic wind profile with

an added stability correction term. The relationship between wind speeds at different heights with stability corrections law is given below:

$$U(z) = \frac{U_*}{k} \ln\left(\frac{z}{z_0}\right) \pm \Psi_m\left(\frac{z}{L}\right) \tag{2.4}$$

Where,

Ψ_m = stability-dependent function

(+) for unstable conditions, (-) for stable conditions, (0) for neutral conditions

L = Monin-Obukhov length L

DNV-RP-C-205 refers to Stull (1988) for the relevant expressions between Ψ_m and L. It was stated that the Monin-Obukhov length L is related to the Richardson number which is a dimensionless parameter whose value determines whether convection is free or forced (Obhrai et al., 2012).

2.4 Atmospheric stability

Stability in the atmosphere can be defined as the tendency of air to resist vertical motion. (Stull, 2000). As a general definition, atmospheric stability refers to the tendency for air parcels to move vertically, either to rise or sink depending on its temperature relative to the surroundings.

To understand this situation, consider the condition that makes air parcel rise (method of lifting) and the type of environment the air parcel is rising through. The environment is characterized in terms of its static stability. Static stability determines whether an air parcel remains buoyant or not. An imaginary parcel of air initially at rest (i.e. static) at some level in the atmosphere when given a slight upward push can either keep rising (unstable case), stay where it is (neutral case) or sink back down (stable case).

One of the most common means of lifting air is referred to as buoyant lifting. When an air parcel at the surface of the earth becomes warmer than the surrounding air, it will become less dense than the surrounding air. The hotter, lower density air will tend to rise, and so it referred to as "buoyant". The air will continue to rise as long as it remains warmer than its environment. Likewise, when a parcel of air sinks, it compresses and the temperature increases.

Turbulence due to atmospheric stability is often referred as buoyancy-generated turbulence. The atmosphere can be classified into three stability classes: stable, neutral, and unstable. Putri (2016) described the main differences between the three classes in Figure 2.5. It is to be noted that the term 'turbulence' refers to summation of mechanically and buoyancy-generated turbulence, unless otherwise stated.

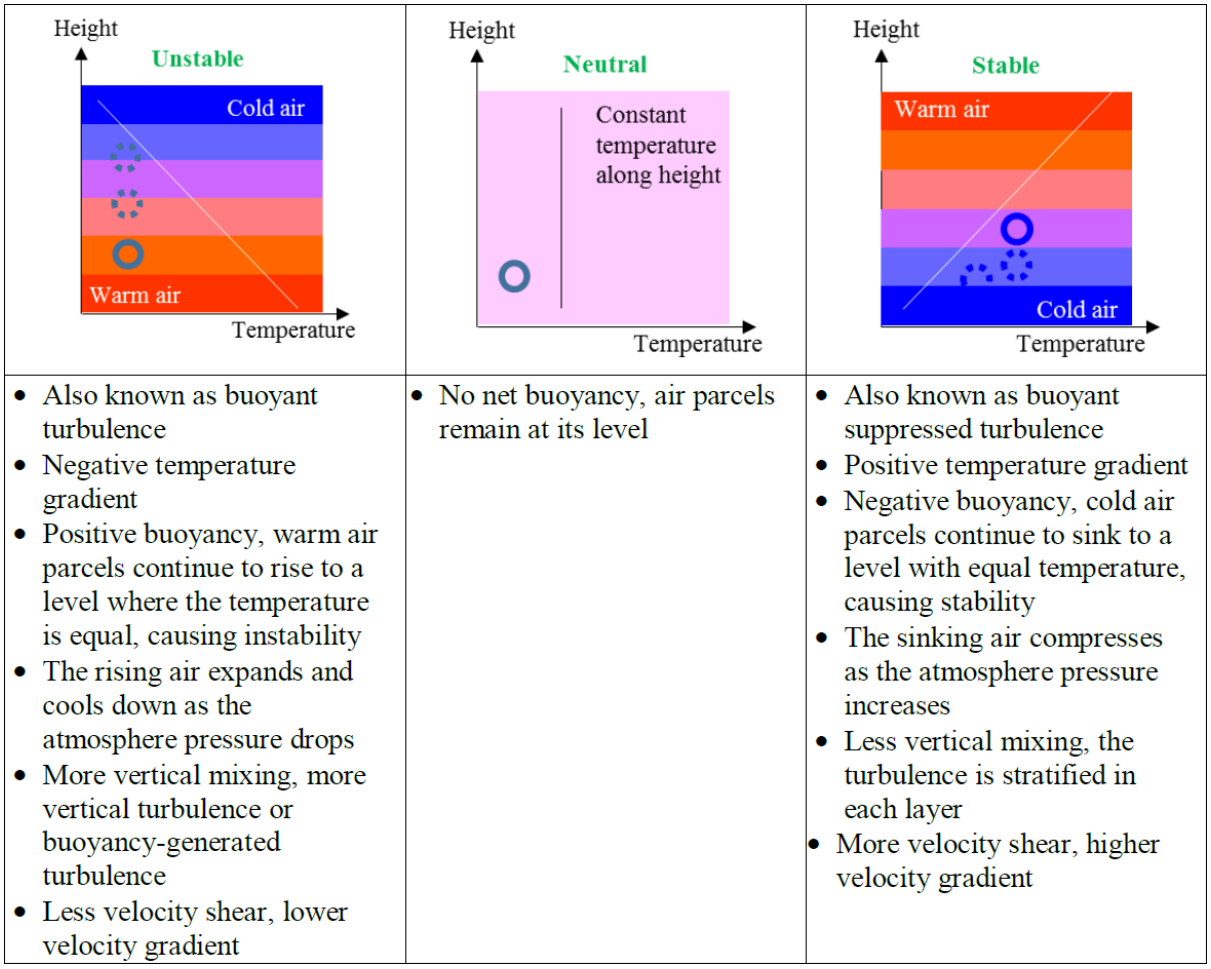

• Also known as buoyant turbulence • Negative temperature gradient • Positive buoyancy, warm air parcels continue to rise to a level where the temperature is equal, causing instability • The rising air expands and cools down as the atmosphere pressure drops • More vertical mixing, more vertical turbulence or buoyancy-generated turbulence • Less velocity shear, lower velocity gradient	• No net buoyancy, air parcels remain at its level	• Also known as buoyant suppressed turbulence • Positive temperature gradient • Negative buoyancy, cold air parcels continue to sink to a level with equal temperature, causing stability • The sinking air compresses as the atmosphere pressure increases • Less vertical mixing, the turbulence is stratified in each layer • More velocity shear, higher velocity gradient

Figure 2.6 Atmospheric stability classes (Putri, 2016).

During the course of day, cooling and heating of the surface of the earth takes place causing different stratification. Stability is determined by the net heat flux to the ground, resulting from the incoming solar radiation and outgoing thermal radiation, and of latent and sensible heat exchanged with the air and subsoil.

On land, the atmospheric stability is a diurnal cycle where stable condition normally occurs at night and unstable condition occurs at around daytime. The heat propagation in the ground through conduction is faster than the heat propagation in the air through radiation, so that during the night, the earth surface is cold, and the atmosphere is still warm from the sun heating at the day. Meanwhile during the day, the earth surface is hot, and the atmosphere is still cold.

Figure 2.7 Diurnal changes in temperature due to heating and cooling at the earth's surface (Jenkins, 2005).

The medium on which heat from the sun travels affects the cycle of atmospheric stability, because of different heat capacity and energy distribution. Offshore, where the surface is water, the cycle of atmospheric stability occurs seasonally. It takes a longer time for the ocean surface to heat up or cool down due to larger heat capacity. Therefore, stable conditions take place during summer (sea surface colder than air), and unstable conditions take place during winter (sea surface hotter than air).

In wind power research, atmospheric stability is usually based on a characteristic length scale called Monin-Obukhov length denoted by L. It can be interpreted as the height above the surface at which turbulence produced by heat conduction first starts to dominate over turbulence produced by shear (Stull, 1988).

As described in Figure 2.6, buoyancy-generated turbulence contributes to air parcel mixing between air parcel layers, so it decreases the wind shear gradient as observed for unstable condition. The opposite effect occurs under stable conditions: the high wind shear, implying abrupt change in wind speed with respect to height (Roy & Sharp, 2013). The effect of atmospheric stability to the mean wind speed profile is shown at Figure 2.8 below.

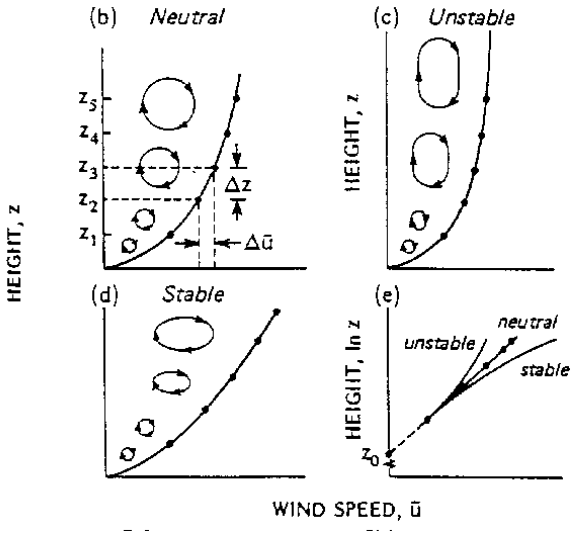

Figure 2.8 Atmospheric stability effect to the mean wind speed profile/wind shear (Thompson, 1979).

The effect of different atmospheric stability on the wind speed profile is apparent from the figure above, so it is necessary to include stability correction on the wind profile calculation, as explained in Chapter 2.3.3. Motta et al. (2005) mentioned the importance of atmospheric stability correction through comparison of estimation and measurements where they found that with the stability correction applied, the error was reduced by 50% (for very stable conditions). Moreover, Ameya et al. (2011) concluded that without stability correction, the measured and estimated wind profile under stable conditions were over-predicted.

2.5 Turbulence

Turbulence influences the yields from wind turbines as well as the loads on wind turbines. Increasing turbulence leads to higher yields and to higher loads, where the latter is more important. Turbulence in the ABL is either generated by shear or by thermal instability. For lower wind speeds, thermal production of turbulence is dominant, but this becomes nearly negligible for high wind speeds when compared to shear production. Emeis (2014) showed that the shear production is proportional to the surface roughness.

Onshore, the shear production is dependent only on the surface roughness and is assumed to be independent from the atmospheric conditions. However, in offshore conditions, surface roughness increases with wind speed and therefore increase the wave height.

2.5.1 Turbulence intensity

Turbulence intensity is defined as the ratio of the standard deviation of the wind speed, σ_u over the mean wind speed $u(z)$. It is to be noted here that σ_u increases with the length of the averaging interval (Emeis, 2012). For a change in the averaging interval from 10 to 30 min the increase is negligible a few metres above ground, because the turbulence length scale is small close to the ground and enough turbulence elements are already contained in a 10-min interval. The increase becomes larger further away from the surface where the turbulence length scale is larger and less turbulence elements pass the measurement instrument in a given time period.

In appendix A of Emeis (2012), a sample from the FINO1 data 80 m above the sea surface showed that σ_u nearly doubled when the averaging period was prolonged from 10 to 30 min.

By using the logarithmic wind profile law, turbulence intensity equation yields as below (Wieringa, 1973):

$$I_u(z) = \frac{\sigma_u}{u_*}\kappa\left(ln(z/z_0)\right)^{-1} = A\left(ln(z/z_0)\right)^{-1} \tag{2.5}$$

Wieringa (1973) set A=1 based on the assumption that the ratio of the standard deviation of the wind speed over the friction velocity, u_*, is $1/\kappa = 2.5$ (Stull, 1988). In principal, Emeis (2014) stated that A should vary with the length of the averaging interval, and the FINO1 data showed values for the ratio σ_u/u_* which were close to 2.5 for wind speeds above 7 m/s using an averaging interval of 10 min.

For onshore, turbulence intensities increase with decreasing wind speeds as stated in IEC 61400-3. In this case the same asymptotic behaviour for low wind speeds is found as over land, leading to higher turbulence intensities (Emeis, 2014). But on the other hand, there is a second influence which is not present onshore: the ocean roughness length increases with increasing wind speed due to the formation of waves (Foreman & Emeis, 2010).

Data evaluation from FINO1 by (Emeis, 2014) shows the relation between turbulence intensity and wind speed at the mean, maximum, minimum, median, 10th percentile, and 90th percentiles. The data used is the measuring period from September 2003 to August 2007 at 90m height at the FINO1. For low wind speeds, the mean turbulence intensity rapidly decreases with increase of wind speed to a minimum value around 4.5% at 12m/s wind speed. Above this minimum, turbulence intensity increases nearly linearly with increasing wind speed. The high turbulence intensity values at wind speeds below about 12m/s originated from the dominance of thermal induced turbulence at low wind speeds during unstable atmospheric conditions with water

surface temperatures significantly above the air temperature. When the wind speed (and so the roughness length) increases further, the mechanical part of the turbulence intensity begins to dominate over the thermal effects and turbulence intensity increases again (Barthelmie, 1999).

2.6 Wind turbine energy output

2.6.1 Weibull distribution

The first step of determining the potential sites for building a wind farm is by identifying the wind energy resource at the site. Therefore, being able to estimate and model the characteristics of the wind energy resource are important in different aspects, including the economic aspect of a wind project. The wind speed is highly variable, both in space and time. In terms of time, the variability can be divided into three time scales (Burton et al., 2001). First, the large time scale variability of the variation of the amount of wind in a year scale, up to decades or more. Second, the medium time scale covering period up to a year, which is more predictable. Monthly variations often used to assess the wind energy potential by statistical analysis of several years measurements of wind speed. Finally, the short-term scale covering time scales of minutes to seconds, known as turbulence, and high frequency wind data captured by wind energy research platform are assessed.

The wind variation for a site in a year period usually described using Weibull distribution, a probability distribution of wind speed, with the detail description can be found in Freris (1990).

Weibull distribution is a two-parameter function often used in statistical analysis, given as below:

$$P(v < v_i < v + dv) = P(v > 0)\left(\frac{k}{c}\right)\left(\frac{v_i}{c}\right)^{k-1} \exp\left[-\left(\frac{v_i}{c}\right)^{k}\right] \tag{2.5}$$

Where c is the Weibull scale parameter, with unit wind speed, k is the dimensionless Weibull shape parameter, v is the wind speed, v_i is a particular wind speed, dv is the wind speed increment. The variation of hourly mean speed around the annual mean is decreasing with the increasing of k, and the variable c shows how high the annual mean speed is. Therefore, in general, a desirable case is having a wind farm site which characterized by high scale factor (c) and a reduced shape factor (k).

2.6.2 Wind turbine power curve

The power curve of a wind turbine is a graph that shows how big the electrical power that can be produced by wind turbine at different wind speeds. There are several points that are important in the power curve such as cut-in speed, rated output power and rated output wind speed, and cut-out speed. Cut-in speed is the wind speed at which wind turbine blade starts to rotate and able to generate power, typically between 3 and 5 m/s depending on the wind turbine design. As wind speed increases the electrical output will rise and when the wind speed reach somewhere between 12 and 17 m/s, the power output reaches the limit and will not be increase anymore, capped by the capability of the electrical generator. This limit is called the rated power output and the corresponding wind speed is called the rated output wind speed. Finally, the cut-out speed is the point at which the the wind speed increases above the rated output such that the braking system of the rotor of a wind turbine is deployed bringing the rotor to a halt thereby reducing risk of damage to the rotor of wind turbine.

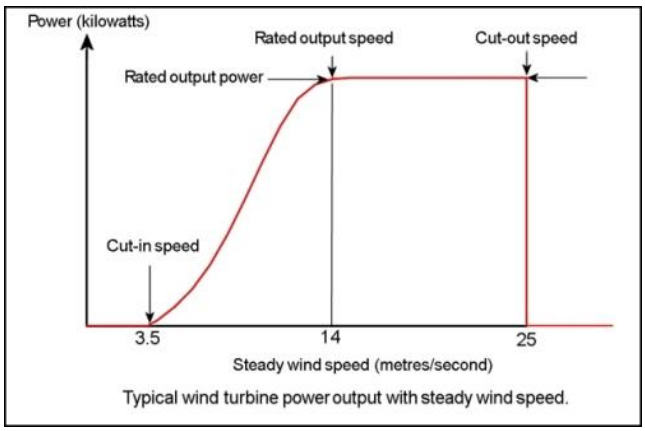

Figure 2.9 Typical wind turbine power curve.

There is a theoretical limit on the amount of power that can be extracted by a wind turbine from wind, which is called Betz limit and by calculation has a value set to 59%.

Power curve design of a wind turbine is made according to several aspects such as the environmental conditions at the site, the wind turbine capability, as well as economic feasibility and profitability. In this study particularly for FINO 1, a German wind farm Alpha Ventus is located in proximity. As a reference of the potential speed requirement regarding wind farm operation near FINO 1, Table 2.2 has been presented below that shows the technical data of typical Alpha Ventus wind turbine related to the power curve and its requirement of wind resource characteristics.

Table 2.2 Technical data related to power curve of a wind turbine in Alpha Ventus wind farm (Bartsch, 2015).

Technical data of Alpha Ventus wind turbine Adwen AD 5-116				
Hub height	Cut-in Speed	Rated Wind Speed	Cut-out Wind Speed	Rated Output
(m)	(m/s)	(m/s)	(m/s)	(MW)
90	3.5	12.5	25	5

In the following sections, the above information is relevant to relate the purpose of FINO 1 research platform instalment, for instance, the fact that the placement of the wind speed measurement is at 90 m. Moreover, as a basis to understand the FINO 1 research, cut-in, rated, and cut-out speed are used as references to implement the wind speed ranges of the result presentation of this study.

2.7 Waves

Waves that look physically similar might have different characteristics depending on how they are generated. Ocean waves are irregular and random in shape, height, length, and speed of propagation. A real sea-state is best described by a random wave model. A linear random wave model is a sum of many small linear wave component with different amplitude, frequency and direction (DNV-RP-C205, 2010).

Stationary sea-state is a common assumption for short term wave condition and can be characterised by environmental parameters such as significant wave height H_s and peak period T_p. Significant wave height is the average of the highest one-third (33%) of waves measured from trough to crest that occur in a given period, whereas peak period is the period of the most energetic wave component.

Wave conditions in a sea-state can be divided into two classes:

- Wind sea/wind wave: waves generated by local wind
- Swell: long period waves generated by distant storms

Wind wave and swells can be distinguished by the ratio of phase speed and wind speed at reference height (usually 10 m) to define regimes of sea-state:

Wave age:

$$\chi_{10} = \frac{C_p}{U_{10}} \tag{2.6}$$

Where,

C_p = phase speed (at the peak of wave spectrum)

U_{10} = Wind speed at reference height 10 m

Table 2.3. Sea State Regime.

Sea State	Wave Age	C	Origin
Growing sea (Young or Developing waves)	< 0.8	Slow	local wind
Mixed sea (Mature waves)	0.8 to 1.2		
Swell (Old waves)	> 1.2	fast	distant storms

Swell waves have longer peak period than wind waves, and swell waves are not locally generated. Therefore, wind wave directionality during swell conditions is interesting since swell can be completely opposing the local wind direction.

2.8 Fetch

Fetch is the distance that indicates how far wind has travelled over open water. For example, if a wind is blowing from east to west across a body of water and there are no obstacles, the fetch of the wind is equal to the east-west distance of the body of water (Bruno, 2017). The term fetch length is mostly used, which is the horizontal distance over which wave-generating winds blow. Fetch length is used in geography and meteorology and its effects are usually associated with sea-state.

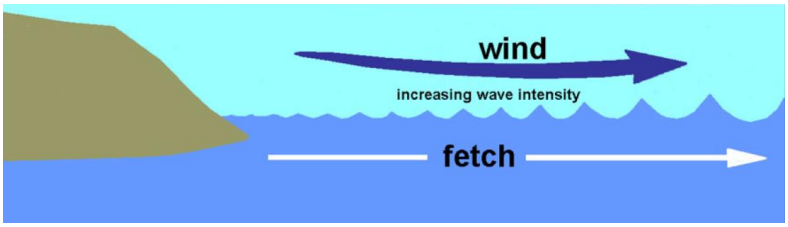

Figure 2.10. Fetch length (Ainsworth, 2006).

Wind and waves are closely related. When wind blows over water friction pulls the surface water along in the same direction. The water gains energy from the wind and waves form because the water is being compressed by the wind.

Once a wave accumulates enough energy and grows to a certain size, it will bump into the wave in front of it which will cause it to gain height. By gaining height a wave exposes its

surface to the wind and gains more energy. This cycle continues to produce larger waves as long as the wind blows in the same direction and there are no obstacles to stop the waves (Bruno, 2017).

Ocean wave intensity reflects the characteristics of wind speed, wind duration, and fetch. There are other factors which can influence the development of a wave field. Some of these include: wind speed and its variation, position and geometry of the coastline, wind direction and water depth. The combinations of these variables lead to a vast number of situations which cannot be simply characterized. Two idealized cases are, however, commonly examined: *fetch limited growth* and *duration limited growth*. Although highly idealized, these cases provide valuable insight into many of the physical processes responsible for wind wave evolution. In addition, they form valuable "test beds" for evaluating the performance of more sophisticated wind wave prediction techniques. These cases also provide estimates of wave conditions which could be expected at a site and are often used in preliminary engineering design (Young, 1999).

To describe the empirical dependences of above topic, Fontaine (2013) states that wind waves are generated and develop with time and space. As the waves grow, wave energy becomes strongly concentrated in the wind direction and is also highly concentrated around a main frequency. The wave system can be described by the peak frequency f_p and the total energy E of its narrow-banded spectrum:

$$E = \overline{\eta^2} = \int_0^\infty \phi(f) df \tag{2.7}$$

Two conditions are important for researchers to examine the surface wave generation exposed to steady wind force. They are fetch- and duration-limited growth condition, which will be explained at the following sub-chapter.

2.8.1 Fetch-limited

Fetch-limited is situation in which wave energy (or wave height) is limited by the size of the wave generation area (Simm et al., 1996).

Young (1999) explains that *Fetch limited growth* occurs when a wind of constant magnitude and direction blows perpendicular to a long and straight coastline. This case is shown diagrammatically in Figure 2.11. The water is assumed deep and the wind blows for a sufficiently long time that the wave field reaches steady state (independent of time). Hence, for

the given wind speed, the wave field becomes a function of the distance from the shoreline, which is termed the *fetch*, *x* (Stiassnie, 2012).

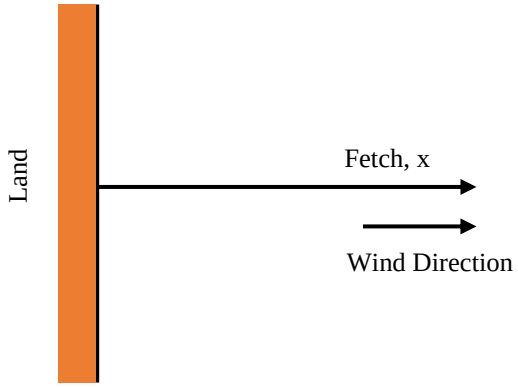

Figure 2.11. Schematic diagram showing fetch limited growth. The wind blows perpendicular to the infinitely long coastline shown to the left. The fetch, *x* is measured offshore in the direction of the wind. For a constant wind speed, the wave field develops as a function of fetch (Young, 1999).

Fontaine (2013) describes that the fetch case corresponds to a steady wind blowing normal to a straight shore and generating an offshore directed forcing as illustrated in Figure 2.12. At a given distance from the shore (fetch), the wind-waves reach a statistically steady state after a long enough time. Assuming that the total energy E and peak frequency f_p depend only on fetch x, wind stress velocity u_0* and gravity g, dimensional analysis enables it to be concluded that:

$$\tilde{E} = \tilde{E}(\tilde{x}) \; and \; \tilde{f_p} = \tilde{f_p}(\tilde{x}) \tag{2.8}$$

where the non-dimensional energy $\tilde{E}$, peak frequency $\tilde{f_p}$, and fetch $\tilde{x}$ are defined as:

$$\tilde{E} = \frac{g^2 E}{u_0^{*4}} \; , \tilde{f_p} = \frac{u_0{}^* f_p}{g} \; , and \; \tilde{x} = \frac{gx}{u_0^{*2}} \tag{2.9}$$

The dependency of the energy and the peak frequency with the fetch has been studied experimentally by numerous researchers. Babanin and Soloviev (1998) and Badulin et al. (2007) provides detailed discussion and comparative analysis of the different fetch laws that have been proposed. As stated by Fontaine (2013), the most well-known dependency is as follow:

$$\tilde{E} \propto \tilde{x} \; and \; \tilde{f_p} \propto \tilde{x}^{-1/3} \tag{2.10}$$

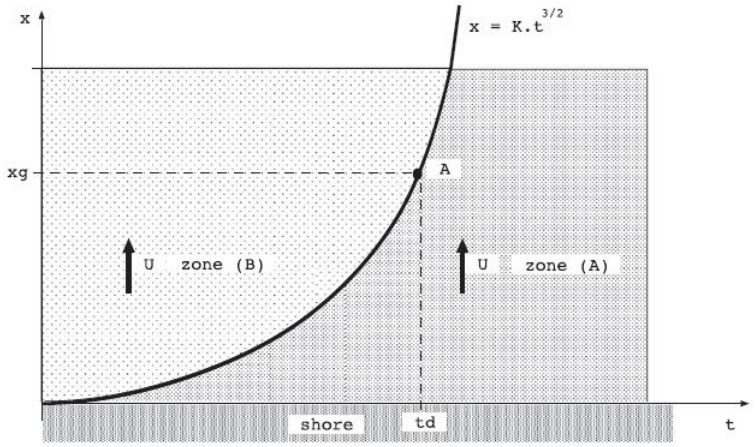

Figure 2.12. Wind is blowing offshore (Fontaine, 2013).

2.8.2 Duration-limited

A related problem to fetch-limited growth is *duration limited growth*. This case considers the development of the wave field from an initially calm sea (Young, 1999). Ideally, the water stays calm until the sudden start of a steady wind reaching rapidly to a set speed. The wind direction may stay steady for a long period of time but ramping up of wind speed from zero to a set speed usually takes some time. Moreover, in the open ocean, background swell is almost always present (Hwang & Wang, 2004).

All land boundaries are assumed sufficiently distant that there is no fetch limitation to growth. The wind field is of constant speed and direction and spatially homogeneous. The water is also assumed to be infinitely deep. For the given wind speed, the resulting wave field will be spatially homogeneous and only a function of the duration or time that the wind has been blowing, *t*. As indicated above, reasonable approximations to fetch limited condition commonly occur, particularly at short fetch. Duration limited conditions are less common and hence the available database is significantly smaller (Young, 1999).

In contrast to the fetch-limited growth, Fontaine (2013) describes that the duration-limited case corresponds to a uniform wind arising at $t = 0$ and blowing over an unlimited fetch far from the influence of the shore. In this case, the wave spectrum at a given time does not depend on the position but only on the duration. As with fetch-limited sea, for limited-duration seas, dimensional analysis enables it to be concluded that:

$$\tilde{E} = \tilde{E}(\tilde{t}) \; and \; \tilde{f_p} = \tilde{f_p}(\tilde{t}), \qquad where \; \tilde{t} = \frac{gt}{{u_0}^*} \tag{2.11}$$

Experimentally, the following relations, also called duration-limited laws, have been proposed:

$$\tilde{E} \propto \tilde{t}^{3/2} \; and \; \tilde{f_p} \propto \tilde{t}^{-1/2} \tag{2.12}$$

The fetch or the duration can be eliminated in equation (2.9) or (2.11):

$$\tilde{E} \cdot \tilde{f_p}^{\,3} = C, where \; C = constant \tag{2.13}$$

Equation (2.12) above has been hypothesized by Toba (1973) and resulting in the relation between significant wave height H_s and wave period T_p:

$$\tilde{H_s} = B \cdot \tilde{T}_p^{\frac{3}{2}}, \qquad where \; B \simeq 6.2 \times 10^{-2} \tag{2.14}$$

This is named *the three-second power law for wind waves of simple spectrum* (Toba, 1973).

In this equation, the non-dimensional significant wave height and wave period are defined as:

$$\tilde{H_s} = \frac{g H_s}{u_0^{*2}} \; and \; \tilde{T}_p = 1/\tilde{f}_p \tag{2.15}$$

However, the assumption of Toba's Law is plausible only within given constraint. For example, Badulin et al. (2007) recover Toba's Law as a particular case of the weakly turbulent law (Fontaine, 2013). The takeaway from above topic that energy increases with fetch or duration is intuitive, considering that energy is transferred from the wind to the waves.

It is informative to see the Hwang and Wang (2004) experimental results of the conversion of fetch-limited to duration-limited growth functions.

3. Previous research on wind-wave misalignment

3.1 Wind-wave interactions

As we can physically understand, the wind blows over the ocean surface and create waves. However, there is condition when the wind is driven by the wave. The wave-driven wind regime is found to be prevalent in the tropics where wind speeds are generally light and swell can propagate from storms at higher latitudes (Hanley et al., 2010). Conversely, the wind-driven wave is occurring in the locations where wind speeds are generally high over the sea. In the open ocean, young wind waves are steeper and can often be higher than old sea or swell. Therefore, young wind waves generally represent a rougher sea surface than the older swells (Janssen, 2004). This sea state dependent roughness can be captured in the Charnock relation (Charnock, 1955).

The roughness length can be considered as the point where the wind speed becomes zero when extrapolated towards the surface using Monin-Obukhov theory (Stull, 1988). Stronger winds produce higher waves and higher sea roughness length. As per DNV-RP-C205, the value of roughness length is generally between 0.0001 m for open sea and 0.01 m for near coastal areas with offshore wind farms.

The roughness length is defined by Charnock relation as below:

$$z_0 = \frac{A_c {U_*}^2}{g} \tag{3.1}$$

Where,

z_0 = roughness length

U_* = friction velocity

A_c = Charnock constant

g = gravity acceleration (9.81 m/s^2)

In a physical sense, roughness length is the smoothness of the terrain contour where wind is blowing. Higher the surface roughness length of a particular surface, more will the wind be slowed down. Table 3.1 showing roughness length of various terrain are presented below.

Table 3.1 Surface roughness length z_0 over various terrain *("Twin Groves: A Lesson in Wind," 2016).*

Terrain Description	**Surface Rougness Length, z (m)**
Very smooth, ice or mud	0.00001
Calm open sea	0.0002
Blown sea	0.0005
Snow surface	0.003
Lawn grass	0.008
Rough pasture	0.01
Fallow field	0.03
Crops	0.05
Few trees	0.1
Many trees, hedges, few buildings	0.25
Forest and woodlands	0.5
Suburbs	1.5
Centers of cities with tall buildings	3

3.2 Causes of wind-wave misalignment

As described in Chapter 2.4, swell is the type of wave that carries high energy, which caused by distant storm, and when local wind blows above the swell, wave-driven wind regime will not be created. In this case we have wind-wave misalignment.

In the idealised wave situation, the mean wave direction is equal to the wind direction. This is consistent with the wave-driven wind logic, which is generated by local winds. However, this is not always the case. The difference between wave and wind direction at a position at sea is seldom equal to zero. There are some physical effects that can cause the mean wave direction to be misaligned with the wind direction. The physical influence includes upwind fetch restrictions, refraction by spatially varying depth and or currents, spatial and temporal variations in the wind field, propagation effects in large areas, parameterization of physical processes, and time step in non-stationary wave model computations (Vledder, 2013).

The phenomenon of upwind fetch restriction could be explained by the fact that to a certain extent, wave growth is directionally decoupled implying that the directional wave spectrum is composed of separate contributions of waves coming from different directions with different fetches and effective wind speeds. In this way upwind variations in fetch result in a mean wave direction that is different from the overall constant wind direction. Upwind variations in fetch make it almost impossible to define a representative fetch for simple wave predictions using parametric methods (Pettersson et al., 2010).

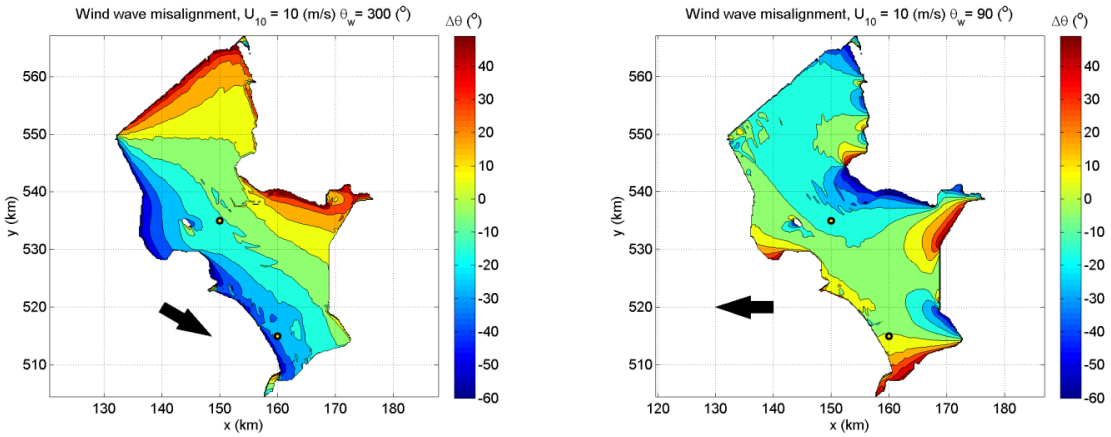

Figure 3.1 Geographical variation of the wind-wave misalignment in Lake IJssel for a situation with a constant northwesterly wind of 10 m/s and a wind direction of 300°N and 90°N (Black arrow) (Vledder, 2013).

The effects on the wind-wave misalignment and on the directional spreading are illustrated for two output locations (shown in the Figure 3.1 as black/yellow circles) in the Figure 3.2.

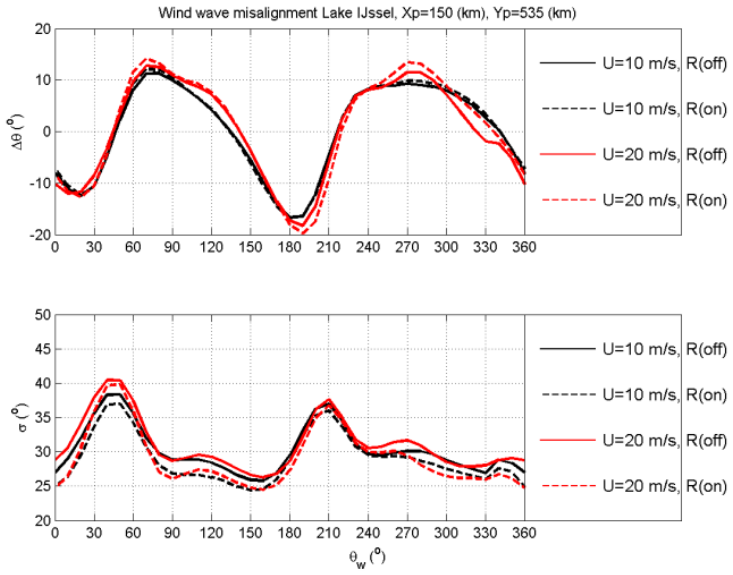

Figure 3.2 Wind-wave misalignment and directional spreading in Lake IJssel as a function of wind direction, and for a situation with (R=on) and without(R=off) refraction activated.

3.3 Magnitude of misalignment

In general, there are misalignments between the wind and waves at all wind speeds: small misalignments at large wind speeds and large misalignments at lower wind speeds (Fischer et al., 2011). Wave heights at real offshore sites tend to diminish with increasing wind/wave misalignment (Barj et al., 2014). The distribution of wind-wave misalignment becomes narrower with increasing wind speed and/or significant wave height (Vledder, 2013).

In this thesis, the magnitudes of misalignment are classified into 4 group:

Table 3.2. Classification of wind-wave misalignment magnitude

Classification / Conditions	**Wind-wave misalignment magnitude (deg)**	**Category**
Aligned	$0 \leq \theta < 30$	*Aligned*
Slightly Aligned	$30 \leq \theta < 60$	*Aligned*
Perpendicular	$60 \leq \theta < 120$	*Misaligned*
Slightly Opposite	$120 \leq \theta < 150$	*Misaligned*
Opposite	$150 \leq \theta \leq 180$	*Misaligned*

To be noted that in this thesis, the magnitude of misalignment is always positive value (absolute value), meaning that the acute angle of the directional difference between wind and wave directions are considered in the analysis. Since long term data is used in this thesis, the chronological misalignment will not be the focus. However, the relative direction can be considered when necessary. Fischer et al. (2011) study the control concept for mitigation of load from misaligned wind and waves on offshore wind turbines supported on monopiles, with the wind-wave misalignment using absolute values from an example site in Dutch North Sea, close to the existing offshore wind farm *Egmond aan Zee (OWEZ)*. The same approach has been used in this study, considering the occurrence of wind-wave misalignment and the relation to turbulence intensity was the research focus. In the other hand, several other researches such as (Kühn, 2001) and (Vledder, 2013) use the range -180 degree to 180 degree of misalignment in their analysis, to consider the direction that causes the misalignment.

3.4 Statistics of wind-wave misalignment

In terms of research and engineering, single events of wind-wave misalignment are not of interest, rather the statistics of wind-wave misalignment. Statistics of wind-wave misalignment can be considered for the total wave system or by breaking down into sea or swell systems. It is expected that, the occurrence of misalignment by swell waves should be higher as swell waves can easily have a different dominant wave direction than the local winds. Wind-wave misalignment has different signatures for wind sea and swell systems, where broader directional distributions are found for swell systems (Vledder, 2013). In a study by (Vledder,

2013), a third-generation wave prediction models WAVEWATCH III (WW3) was used to perform wave model based on hindcast, in order to compare the observed and predicted mean wave direction.

Vledder (2013) mentioned that the sea-distribution is much narrower than the total wave system and the swell system. As expected, the distribution of the swell waves is the broadest as swell waves have a different dominant wave direction than the local winds. Figure 3.4 below is a graphical representation of the wind-wave misalignment for the total wave field, the wind-sea part, and the swell part in the north-west Australian continental shelf.

A result by Vledder (2013) for a wind-wave misalignment located on the north-west Australian continental shelf show that most of the events occur in the difference band from -10° to 10°, slowly becoming smaller with increasing directional difference. Moreover, distribution of wind-wave misalignment becomes narrower with increase of wind speed and significant wave height (Vledder, 2013).

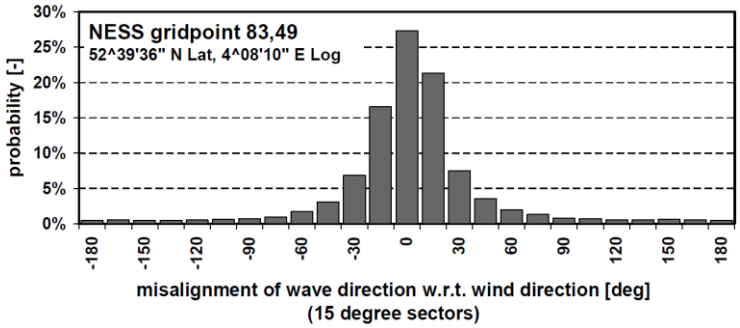

Figure 3.3 Misalignment of mean wave w.r.t. mean wind direction at a Dutch North Sea site (Kühn, 2001).

From the database of North European Storm Study (NESS), data for two grid points in a Dutch North Sea site is checked for a continuous record of 9 years. As seen from Figure 3.3 above, the misalignment observation of mean wave direction with respect to mean wind direction at this site suggest that misalignment of up to 30 deg is common, while misalignment larger than 60 deg occurs less than 5% of the time (Kühn, 2001).

3.5 FINO 1 research platform related research

FINO 1 research has been conducted not long after its operation and a long-term data analysis has been performed to a certain extent. Kettle (2013) was explaining from the basis of how the government policy and background is originated, the design, instrument array, data logging, and communication, as well as the recognized problems in the FINO data set. Some insights that might garner interest in this thesis are mast flow distortion, wind direction, anomalies in the logging system for the slow and fast meteorological data, and most importantly the data gaps from instrument malfunction, power loss, and computer failure, which will be related directly to the data gathered for the long term FINO 1 analysis conducted in this study. As for the latter, some instruments have been detected to be more vulnerable to damage in the extreme environment compared to the others. For instance, during the first winter of its operation, there was damage to the central chain of oceanographic instrument during a storm in December 2003. Therefore, it can be expected for either a lack of data or non-continuous data set in this period owing to the fact that most of the data were slow profiling met-ocean instruments, except the sonic anemometers, and were archived with 10-min average. Wind speed is an exception because it has good records of standard deviation, along with the minimum and maximum values over 10 minutes interval which later can be used to evaluate the turbulence intensity. In terms of the wave rider buoy, there is important measurement in the high frequency data recording that is lost in the long-term average statistics. The original high frequency data recordings from the slow-profiling instruments at FINO 1 have been lost for the period before 2006. This fact is the main reason that the data set processed in this thesis starts at 2006.

Another more detailed research in relation to data processing on FINO 1 data set was performed by (Westerhellweg et al., 2010), who assessed the uncertainty of mast correction in respect to wind shear as well as the wind direction and wind speed dependency of the turbulence intensity. There are more dynamics to be considered by installing research platform at offshore, such as the lateral speed-up effects, upwind flow retardation, and downwind wake effects. The combined wind and wave loads create the necessity to employ different mast designs, which may result in shorter booms as compared to onshore masts. The disturbances caused by the masts was addressed by developing a mast correction method called “uniform ambient flow mast correction”, UAM (Neumann, 2007). In order to investigate the mast correction issue, additional top anemometer was installed at a 104.5 m LAT height. The ratio of the wind speeds of this additional anemometer and the top anemometer at 103 m was presented by (Westerhellweg et al., 2012). The result shows the flow distortion of the booms at wind

directions 0°, 90°, 180°, and 270°. Constant speed-up effects are present for the original top anemometer for the wind direction sectors between those directions, which is the effect of the presence of lightning cage installed at the top of the mast.

Therefore, mast correction was evaluated for the unstable data set and V_{boom} which is the wind speed corrected according to the wind shear was introduced. It has been found that the higher mast correction is concentrated on a certain range of wind direction, north-west direction for cup anemometers and south-east direction for sonic anemometer. Those are in fact the disturbed direction, opposite to the orientation of the boom from the mast of both instruments which are described in detail at the next chapter, see Table 4.2 and Table 4.3. As reference to analyse the data in this thesis, the mast correction and its uncertainty were displayed by (Westerhellweg et al., 2012) and it was shown that the FINO 1 cup anemometers have the highest mast correction in the range of wind direction 300° to 360°. Meanwhile the highest mast correction for sonic anemometers in the range of wind direction 100° to 150°. However, the uncertainty of the mast correction was caused by several other sources such as wind shear, and stability effects. Finally, the overall uncertainties were calculated from the combination of sources and the outcome can be seen in Table 3.3 below. This previous research is important to understand because this become one consideration of choosing a certain height for data analysis in this thesis.

Table 3.3 Overall uncertainty of mas correction wind speeds for FINO 1 (Westerhellweg et al., 2012).

Anemometer	Overall uncertainty of mast correction
Cup 104.5	2%
Cup 91.5	2%
Cup 81.5	2%
Cup 71.5	3%
Cup 61.5	3%
Cup 51.5	3%
Cup 41.5	4%
Sonic 81.5	2%
Sonic 61.5	2%
Sonic 41.5	3%

Another research that would be an interest in relation to this thesis was the dependency of turbulence intensity on wind direction and wind speed. FINO 3 shows big differences of the turbulence intensity for different wind directions, although in FINO 1, it is more homogeneous. (Westerhellweg et al., 2010). However, in this thesis, the dependency on wind speed has been

observed in more detail since the OBLEX data for lower heights wind speed are going to be introduced later and offshore wind profiles in regard to wind-wave misalignment are presented as a result. According to the previous research source, the average turbulence intensity has a minimum at approximately 11 m/s and increases for higher wind speeds as shown in Figure 3.4. This result is in agreement with the result of this thesis as shown in Figure 5.28 and Figure 5.29, while the difference is that the turbulence intensity was assessed more towards the effect regarding wind-wave misalignment.

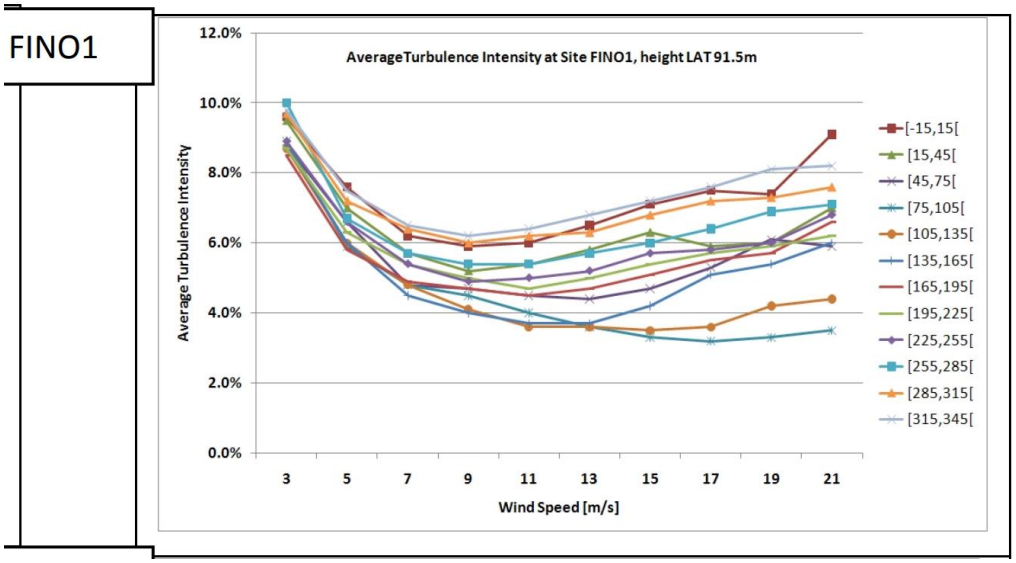

Figure 3.4 Average turbulence intensity for the different wind directions at FINO1 (Westerhellweg et al., 2010).

4. Methodology

4.1 Research platforms

There are two research platforms, FINO 1 and FINO 3, and one additional measurement campaign, OBLEX, located in North Sea which are the main input data used in this thesis. FINO stands for *Forschung In Nord und Ostsee* (Research at North and Baltic Sea) and financed by the German Federal Environmental Ministry. This research was aimed to install research platforms close to future offshore wind farms with the purpose to investigate the environmental offshore conditions as well as creation of comprehensive meteorological, hydrographical, technical and biological data base (Beeken & Kindler, 2011).

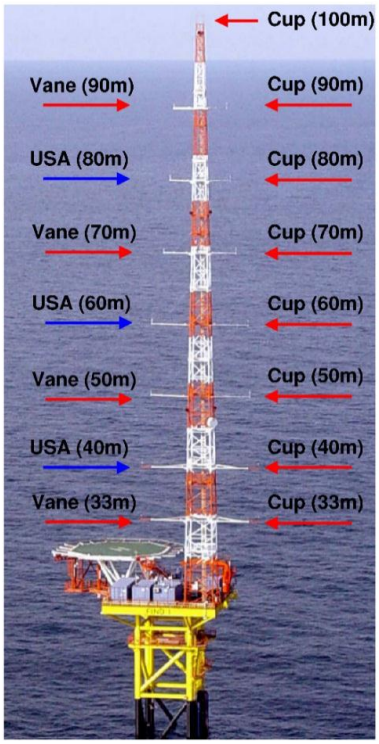

Figure 4.1. FINO 1 offshore research platform instruments (Ernst & Seume, 2012)

4.1.1 FINO 1

FINO 1 is located at North Sea, approximately 45 kilometres to the north of Borkum, in a depth of around 30 metres of water. The site of Alpha Ventus, the first German offshore wind farm, consisting of twelve wind turbines which have been generating power since April 2010, is in the immediate vicinity. FINO 1 was brought into service in the autumn of 2003.

The mast is positioned 33 m from the lowest astronomical tide (LAT), and the height of the mast is 103 m. The mast is equipped with cup anemometers, ultrasonic anemometers (USA), wind vanes and temperature measurements. It measures wind speed at 8 different height from 33 m to 100 m as shown in Figure 4.1. The buoy and AWAC are measuring the wave height, wave direction, and wave peak period with 30 minutes and 1-hour period.

The measurement setup is arranged according to FINO 1 mast shape which is a square cross-section. Cup anemometers are installed on booms on the south-east side of the mast, while the main wind direction is south-west. Wind vanes and ultrasonic anemometers are installed on the opposite north-west side of the mast, as can be seen in Figure 4.1 as well. The boom lengths vary from 3 m to 6.5 m. The ratio of the boom lengths to the mast width varies from 2.2 to 2.7 (Westerhellweg et al., 2012), refer to Table 4.1 below.

Table 4.1 Dimension of FINO 1 masts and booms (Westerhellweg et al., 2012).

Anemometer, height LAT	Mast width	Boom length	Orientation	Ratio (distance to mast centre/mast width)
(m)	(m)	(m)	(°)	(-)
cup 91.5	1.375	3	135	2.7
cup 81.5	1.754	3	139	2.2
cup 71.5	2.124	4	143	2.4
cup 61.5	2.504	5.5	142	2.7
cup 51.5	2.875	5.5	140	2.4
cup 41.5	3.254	6.5	142	2.5
cup 34	3.532	6.5	143	2.3
sonic 81.5	1.754	3	311	2.2
sonic 61.5	2.504	5.5	308	2.7
sonic 41.5	3.254	6.5	308	2.5

The cup anemometers have three conical shells that move around a vertical axis upon on wind speed that blows through it. Then, the rotation is transmitted to the axis and converted into an electrical signal. This instrument is operating at 1 Hz, therefore will capture the wind speed once every second. Image of the cup anemometer and its technical specifications can be seen in Figure 4.2 and Table 4.2 below.

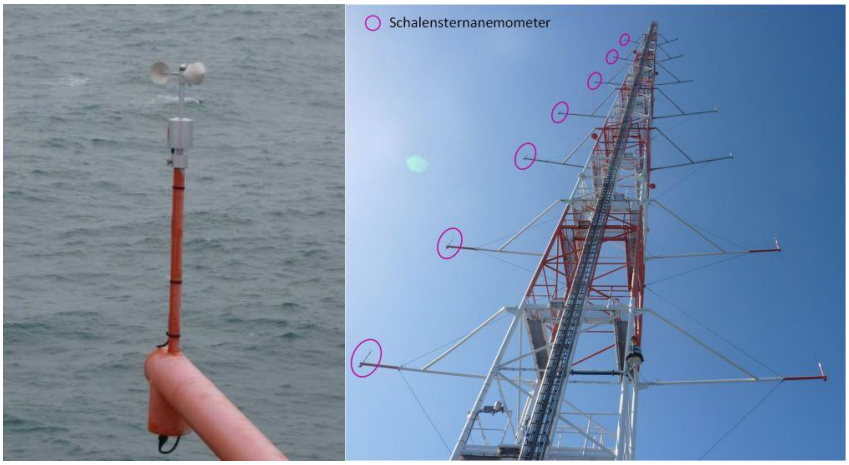

Figure 4.2 FINO 1 cup anemometer (Bundesamt für Seeschifffahrt und Hydrographie, 2018).

Table 4.2 FINO 1 cup anemometer specifications (Bundesamt für Seeschifffahrt und Hydrographie, 2018)

FINO1 cup anemometer technical specifications	
Manufacturer	Vector Instruments
Measuring range	Type A100LM up to 75 m / s Type A100LK up to 150 knots

Resolution	Distance constant 2.3 m + - 10% Type A100LM 0.1 m Type A100LK 0.0515 m
Measuring interval	1 Hz
Log interval	1 min
Height	**Orientation to boom from the mast**
101 m LAT	Top
91.5 m LAT	135 °
81.5 m LAT	139 °
71.5 m LAT	143 °
61.5 m LAT	142 °
51.5 m LAT	140 °
41.5 m LAT	142 °
34 m LAT	143 °

Figure 4.3 Vector instruments A100 series cup anemometers (Windspeed Limited, 2018).

The other instruments on the mast that capture wind speed are ultrasonic anemometers (USA), which located on the opposite side of the mast to the cup anemometer as shown in Figure 4.4. These instruments operate by using 3 sound transmitter and receivers which are aligned in pairs opposite to each other into three spatial directions. The transmitted sound waves are displaced by the wind and reach the receiver with a certain time delay. The horizontal wind speed and wind direction are calculated from the wind speeds along the three-spatial axis by derivation from the time delay. Compared to the cup anemometer, ultrasonic anemometer has higher measurement frequency at 50 Hz, meaning that it captured the wind speed 50 times every second and is expected to have more precise measurement. The technical specifications of the ultrasonic anemometers can be seen in Table 4.3.

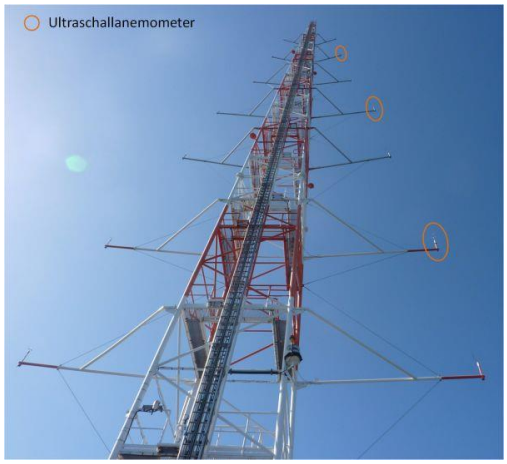

Figure 4.4 FINO 1 ultrasonic anemometer (Bundesamt für Seeschifffahrt und Hydrographie, 2018).

Table 4.3 FINO 1 ultrasonic anemometer specifications (Bundesamt für Seeschifffahrt und Hydrographie, 2018).

FINO1 ultrasonic anemometer technical specifications	
Manufacturer	Gill Instruments R3-50
Measurement range	0-45 m/s
Resolution	0.01 m/s and 1°
Measurement interval	50 Hz
Logging interval	10 Hz
Height	**Orientation to boom from the mast**
81,5 m LAT 61,5 m LAT 41,5 m LAT	311° 308° 308°

As can be seen from the specifications, the cup anemometers cover all the height in consideration (30-100 m) with orientation around 140 degrees and can be considered as South-East (SE) direction, whilst the ultrasonic anemometers cover the height 40 m, 60 m and 80 m with orientation around 310 degrees and can be considered as North-West (NW) direction. This information will be important regarding the following chapter, in terms of distinguishing the good data and the bad data. The wind speed measurements will be selected according to the wind direction, to make sure that the processed data has no disturbance effect caused by the mast tower.

The wind direction of horizontal wind speed is measured by wind vane, and the technical specifications have been presented in Table 4.4. Deflection of the wind vane axis by the wind is transferred to a circular potentiometer to give the resulting wind direction.

Table 4.4 FINO 1 wind vane specifications (Bundesamt für Seeschifffahrt und Hydrographie, 2018).

FINO1 wind vane technical specifications	
Manufacturer	Adolf Thies GmbH & Co.KG
Threshold	0,5 m/s
Measurement interval	1 Hz
Logging interval	1 min
Height	**Orientation on boom off mast**
91,5 m LAT	315°
71,5 m LAT	307°
51,5 m LAT	310°
34m LAT	307°

Another device is the wave rider buoy shown in Figure 4.5 which follows the sea surface movement and measures the wave height by calculating the vertical/horizontal acceleration of the buoy. The FINO 1 buoy is placed close to the platform (approximately 200 m) and transfers the ocean wave data by radio link connection to the data acquisition system at the station. The Datawell wave rider buoy is also used to transmit the additional wave parameters such as significant wave height, maximum wave height, wave period, wave direction and data set of temperature near the sea surface.

Figure 4.5 Recovery of a wave rider buoy (Bundesamt für Seeschifffahrt und Hydrographie, 2018).

4.1.2 OBLEX-F1

In May 2015, NORCOWE started up an extensive offshore measurement campaign at the German research platform FINO1 close to the Alpha Ventus wind farm. This campaign, called

OBLEX-F1 (Offshore Boundary-Layer Experiment at FINO1), took place between May 2015 to September 2016. The research platform is located in the German sector of the North Sea, approximately 45 km off the German Island Borkum.

There are three main instruments in OBLEX-F1 (Flügge & Løvset, 2018):

- Two 3D scanning LiDAR systems which were installed inside the met-mast on top of an additionally installed container, respectively.
    - The first LiDAR system installed inside the met-mast performed Plan Position Indicator (PPI) and Range Height Indicator (RHI) scans towards the south-eastern part of the Alpha Ventus wind farm. Located at 20 m LAT.
    - The second LiDAR system was installed on top of a 10-foot container, which was installed between the met-mast and the FINO1 crane on the south-east side of the platform for the OBLEX campaign. This LiDAR system performed both PPI and RHI scans towards the AV4 wind turbine, in addition to vertical wind profile (DBS) scans. Located at 25 m LAT.
- Two sonic anemometers.
    - The device type is Gill R3-100.

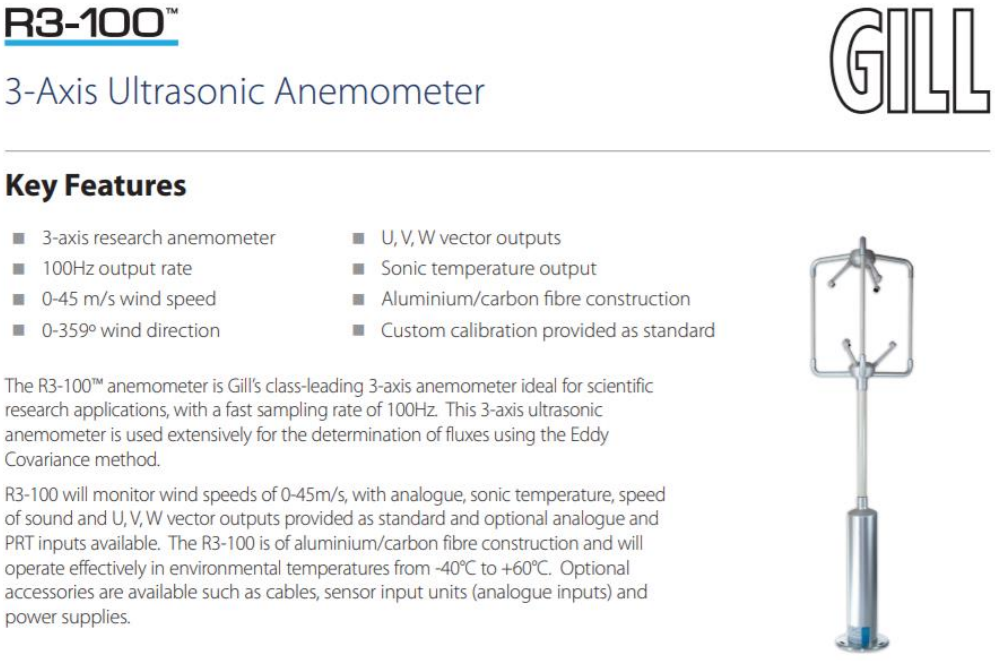

Figure 4.6 Gill R3-100 Ultrasonic Anemometer Specifications (Gill Instruments Limited, 2013).

    - Sampling frequency was set to 25Hz.

  - The axis orientation was set to SPAR, i.e U-velocity is in line with the main spar when viewed from above.
  - The main SPAR (x-axis / U-vel.) is pointed out and away from the platform, i.e. towards SE, 135 deg.
  - The U-vel and V-vel are negative when the wind blows towards the respective coordinate axes, and positive when the wind blows away from the respective anemometer coordinate axes.
  - The sonic anemometers were installed on two temporarily outward facing booms facing toward south-east (135°).
  - The booms were attached to the railings at the platform deck (20 m LAT) and the round walk (15 m LAT).
  - The measurement height of the sonic anemometers were 15.5 m LAT and 19.5 m LAT respectively.
- Radiometer.
  - The passive microwave radiometer was installed on top of FINO1 outermost generator container on the western corner of the platform.
  - This instrument performed passive measurements of incoming radiation in the K-band (22 – 31 GHz) and V-band (51 – 58 GHz) in order to obtain vertical profiles of temperature and humidity.
  - The radiometer was installed at a height of 25m LAT.

Figure 4.7 NORCOWE OBLEX-F1 Campaign Instruments (Flügge, 2018).

The key purpose of the campaign is to add to the knowledge of the marine boundary layer stability, air-sea interaction and offshore wake propagation effects. The collected observational data aids to validate and improve numerical models and tools for i.e. weather forecasting, marine operations, power performance and wind farm layout (Svardal, 2015).

For reference and validation of wind measurements, the FINO 1 metmast, in which the OBLEX campaign was carried out, is equipped with cup, vane and sonic wind sensors up to 100m. Two sonic anemometers (DCF systems) were mounted under the met mast at approximately 15 and 20 m LAT to expand the turbulence characterisation capability at FINO1 and provide wind measurements closer to the sea surface (Svardal, 2015).

4.1.3 FINO 3

FINO 3 is located about 45 miles (80 kilometres) west of Sylt at the edge of the area potentially suitable for wind turbines before the Schleswig Holstein North Sea coast. The approved offshore wind farms Sandbank 24, Nördlicher Grund, DanTysk and OSB Butendiek lie in the near vicinity. FINO 3 was brought into service by the end of August 2009. The mast is equipped with cup anemometers, ultrasonic anemometers, wind vanes, thermometer/hygrometer and pressure measuring tools. It measures wind speed at 8 different height from 30 m to 100 m as

shown in Figure 4.8. The buoy and AWAC are measuring the wave height, wave direction, and wave peak period with 30 minutes and 1-hour period.

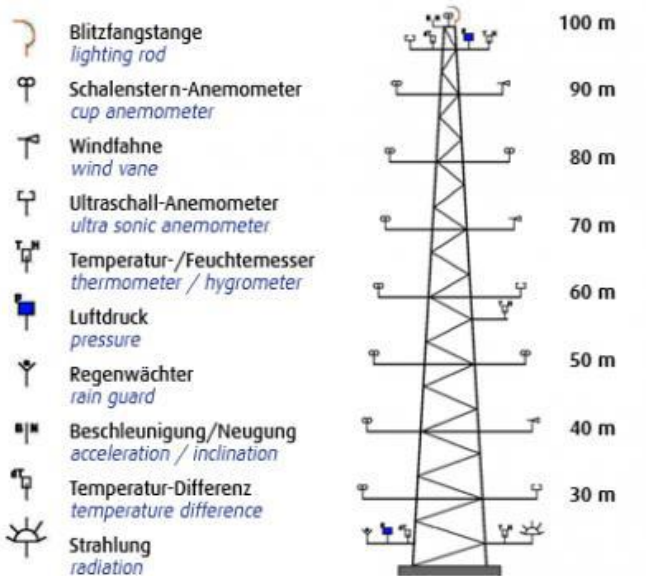

Figure 4.8. FINO 3 offshore research platform instruments ("Meteorologie," 2017).

As FINO 3 was brought into service 6 years after FINO 1, there was an improvement made to reduce the significant flow distortion that occurred in FINO 1. This was done by changing the mast shape into triangular base, as illustrated in Figure 4.9 below.

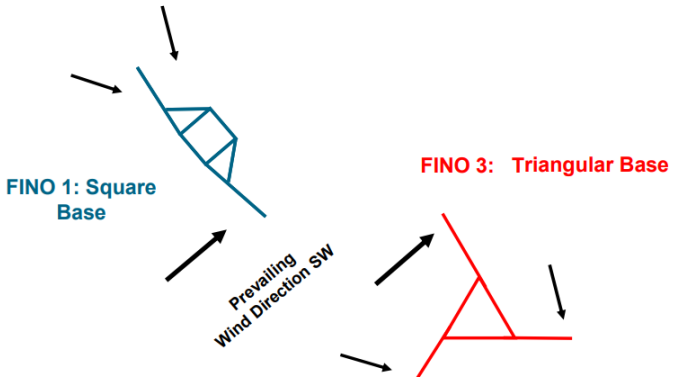

Figure 4.9 FINO platforms top view mast arrangement (Beeken & Kindler, 2011).

Further adjustment was made in this thesis regarding data acquisition in relation to this mast arrangement, see the following Chapter 4.2. Moreover, summary of the technical facts of FINO platforms is presented at Figure 4.5 below.

Table 4.5 FINO Research Platform technical facts (Beeken & Kindler, 2011).

Research Platform	Location	Commissioning	Height	Water depth	Distance from coast	Foundation	Platform size
FINO 1	North Sea	September 2003	101 m	28 m	45 km	Jacket	16*16 m
FINO 2	Baltic Sea	May 2007	101 m	24 m	31 km	Monopile	12.2*12.2 m
FINO 3	North Sea	August 2009	120 m	23 m	80 km	Monopile	13*13 m

4.2 Assumptions

There are several assumptions used in analysing the FINO 1 and FINO 3 data, summarised as below:

- Wind and wave direction data are in the direction of coming to the mast (direction of the instrument receiving data is towards the mast).
- Peak wave period Tp is used to distinguish the swell and wind-wave condition, for checking the wind-wave misalignment under swell and under wind-wave.
    - Swell condition: $Tp > 10$ s
    - Wind-wave condition: $0 < Tp < 10$ s
- Wind-wave misalignment in each FINO 1 and FINO 3 was done by using wind direction at 90 m as it was found to be the most complete data (Kettle, 2013) and most resembles the hub height of wind turbine.
- Processed data for occurrence of wind-wave misalignment are wind speed 90 m height, wind direction 90 m height, and buoy wave direction, for both research platforms. Exception for FINO 1 where the wind speed 80 m height was used to take into account the disturbance effect.
- Wind data measurements were selected for the analysis based on the undisturbed wind direction. For FINO1, there are 2 side of masts sitting on different booms in two opposite directions. This leaves a valid measured zone for each instrument, as illustrated in Figure 4.10 below. As explained at subchapter 4.1.1, the wind direction 240° to 30° will be extracted from ultrasonic anemometer data (boom direction around 310°) and the wind direction 30° to 240° will be extracted from cup anemometer data (boom direction around 140°).

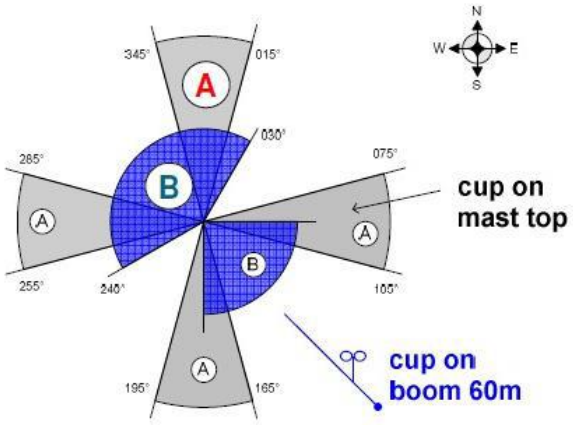

Figure 4.10 Arrangement of FINO1 instruments placement (wind vane, cup and ultrasonic anemometer).

- For FINO 3, it was designed with triangular base that have three booms to minimize the effect of distortion, see Figure 4.12. There are three booms of 105°, 225° and 345° which lead to six sectors in the circular pie that represents the undisturbed sectors captured by each mast. Refer to Figure 4.11 below for the illustration of undisturbed sectors of each mast. The FINO 3 data processed in this thesis were selected according to these sectors.

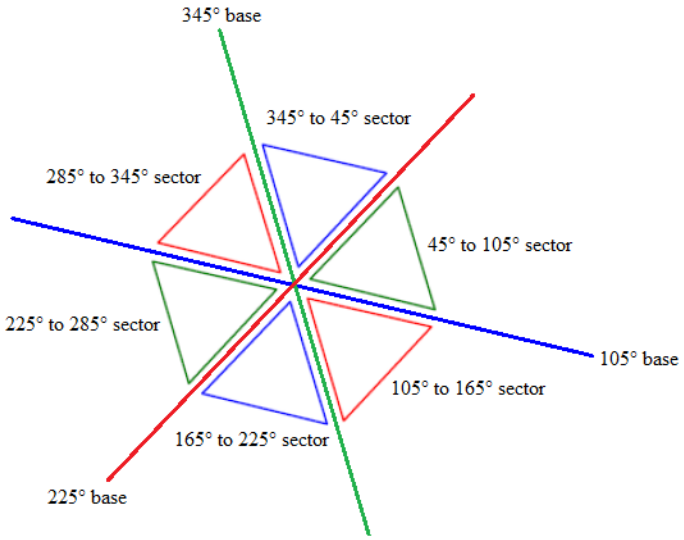

Figure 4.11 Undisturbed sectors in FINO 3 masts.

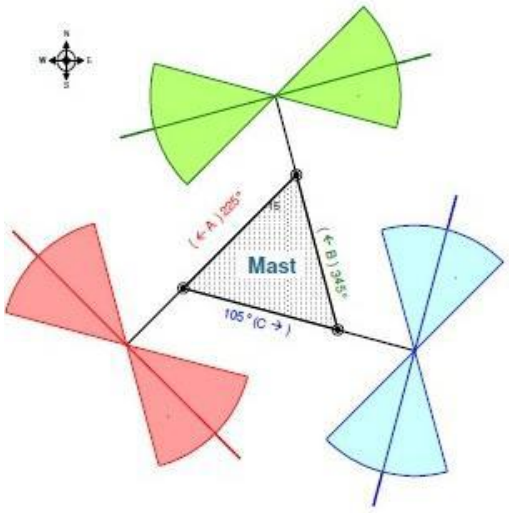

Figure 4.12 Mast shape arrangement of FINO 3 (cup and ultrasonic anemometer, wind vane).

The assumptions used in analysing the OBLEX data are summarised below:

- One month of data was taken from the NORCOWE Data Extraction Portal, the period is from 15 September 2015 to 15 October 2015 for the 15 m and 20 m heights. This period was chosen by considering the best data availability to the corresponding higher measurement data at FINO 1.
- The available data were in three-dimensional wind speed U, V and W direction
- The wind direction was determined by calculating the resultant wind speed from U-wind speed and V-wind speed, and then calculate the resulting angle.
- Analysis in the result chapter was done by taking the OBLEX data at the same direction sector with FINO 1 data, to ensure that they are valid data to be combined.
- There were some issues regarding non-regular measurement interval and some repeating values. This was addressed by adding NaN values (Not-a-Number) in appropriate places and interpolating onto a regular grid.

4.3 Long-term data sets

The long-term data sets from FINO 1 and FINO 3 in this thesis were taken from the official BSH database website, http://fino.bsh.de, originally in the format of '.dat'. These data are under supervision of DEWI. Refer to Figure 4.13 below.

Figure 4.13 Download section of FINO 1 and FINO 3 database (Bundesamt für Seeschifffahrt und Hydrographie, 2018).

The high frequency data sets from OBLEX-F1 were taken from the official NORCOWE OBLEX-F1 web portal, http://www4.cmr.no:5000, originally in the format of '.nc'. This data is under supervision of NORCOWE. Refer to Figure 4.14 below.

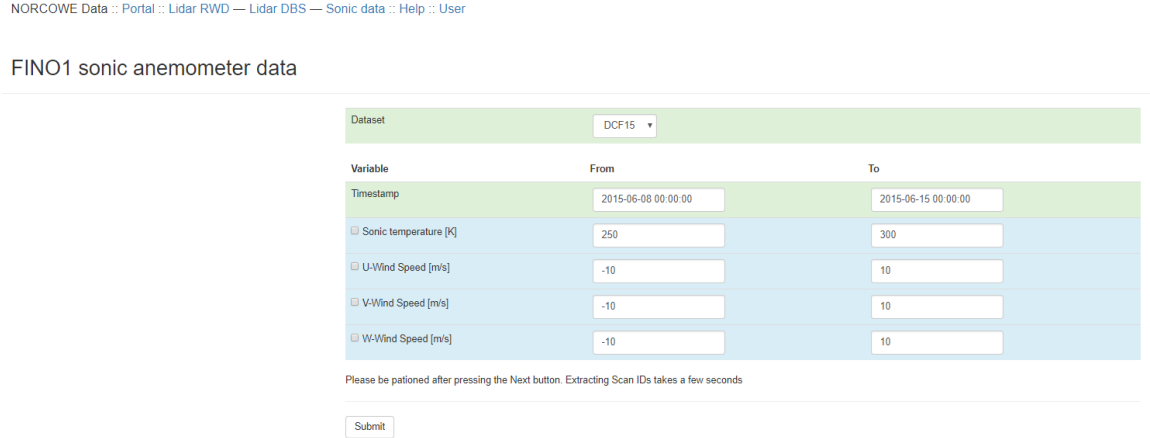

Figure 4.14 Download section of OBLEX F-1 database (NORCOWE, 2018).

4.3.1 FINO 1

The long term FINO 1 data set used in this study is 11 years of data at a 10-minute interval, stretching from 1st January 2006 00:00 to 1st October 2017 00:00, with total data points 617,903 records. The data availability has been discussed below:

- Available data of wind speed at assumed hub height 90 m is 585,980 data points, resulting in a 94.83% data return for wind speed at 90m height.
- However, after removing data due to the mast distortion effect as described in Chapter 4.2, *valid data* of wind speed at assumed hub height 90 m is 344,070 data points, resulting in a 55.68% data return for undisturbed wind speed at 90m height. The wind speed data at 80 m was eventually used because the data return was observed higher at 88.1%, see table Table 4.6 below.
- Available data of wind direction at assumed hub height 90 m is 584,653 data points. Resulting in a 94.62% data return for wind direction at 90m height.
- Available data of buoy wave direction is 448,335 data points, resulting in a 72.56% data return for buoy wave direction. To be noted that the initial data of the wave direction was at 30 minutes interval, so the data was interpolated to a 10 minutes interval to match with the wind direction data. The lower data return for the buoy wave direction happened because there were several time periods when the wave buoy was not activated, according to the report of FINO 1 by Anthony Kettle (Kettle, J., 2013).

Table 4.6 FINO 1 data return.

Data Return of FINO 1	**11 years Available Data**	**11 years Valid Data (Undisturbed)**
Wind Speed Height 90 m (%)	94.83%	55.68%
Wind Speed Height 80 m (%)	88.1%	88.1%
Wind Direction Height 90 m (%)	94.62%	
Wave Direction Buoy (%)	72.56%	

4.3.2 OBLEX

OBLEX data set used in this study is 1 month of high frequency data at 25 Hz. The period is from 15th September 2015 00:00 to 15th October 2015 00:00. There are two sonic measurements data at 15 m LAT and 20 m LAT. Despite the OBLEX data only covers 1-month period, the high frequency data of 25Hz results in a huge 64,800,000 data points, but there were in fact 64,763,712 total data points for sonic anemometer 15 m height and 64,610,955 total data points for sonic anemometer 20 m height.

The data availability has been discussed below:

- Available data of wind speed at 15 m height is 64,504,867 data points, resulting in a 99.83% data return.
- Available data of wind speed at 20 m height is 64,688,169 data points, resulting in a 99.88% data return.
- However, the wind speed at undisturbed directions (30°-240°) was selected, and available data was found to be 73.22% at 20 m height and 63.82% at 15 m height.

Table 4.7 OBLEX data return.

Data Return of OBLEX	**1-month Available Data**	**1-month Valid Data (Undisturbed)**
Wind Speed Height 15 m (%)	99.83%	63.82%
Wind Speed Height 20 m (%)	99.88%	73.22%

4.3.3 FINO 3

The long-term FINO 3 data set used in this thesis is 8 years of data at a 10-minute interval, stretching from 1st October 2009 00:00 to 2st October 2017 00:00, with total 420,769 data points. The data availability has been discussed below:

- Available data of wind speed at assumed hub height 90 m is around 401,688 data points, resulting in a 95.47% data return.

- However, after removing data due to the mast distortion effect as described in Chapter 4.2, *valid data* of wind speed at assumed hub height 90 m is 384,621 data points, resulting in a 91.41% data return.
- Available data for wind direction at a height of 90 m is 379,078 data points. Resulting 90.09% data return for wind direction at 90 m height.
- Availability of the buoy wave direction is 367,440 data points, resulting in 87.33% data return. To be noted that the initial data of the wave direction was at 30 minutes interval, so the data was interpolated to a 10 minutes interval to match with the wind direction data.

Table 4.8. FINO 3 data return.

Data Return of FINO 3	8 years Available Data	8 years Valid Data (Undisturbed)
Wind Speed Height 90 m (%)	95.47%	91.41%
Wind Direction Height 90 m (%)	90.09%	
Wave Direction Buoy (%)	87.33%	

4.4 Analysis method

The meteorological data from FINO 1 and FINO 3 platforms in the North Sea for the 11-year and 8-year time period respectively were studied in order to compare the wind-wave misalignment conditions at the two different locations. Wind speed and wind direction were fitted to have data record with 10 minutes interval. However, particularly for OBLEX data, there are several range of data points which are not exactly at 25 Hz (bad data), meaning that the interval can be less or more than 40 milliseconds at a certain time. This issue has been resolved by doing a linear interpolation across the datasets. The wave rider buoy data were originally at 30-minute. The wave data has been fitted to the 10-minute interval to correlate with the wind speed and wind direction.

Matlab R2016b and Microsoft Excel 2010 have been used to process the data sets as well as producing the result in plots and charts at the following chapter.

5. Results

5.1 General metocean conditions

The meteorology and oceanography (metocean) conditions of FINO 1 and FINO 3 are directly related to their location in the North Sea. FINO 1 and FINO 3 are 136 km apart, with FINO 1 situated approximately 45 km from the shore, and FINO 3 situated approximately 80 km from the shore. In relation to fetch as explained in Chapter 2.7, FINO 3 has roughly twice as long fetch compared to FINO 1, which together with wind speed, directly affects the size (sea state) of the waves recorded. Moreover, according to the research by Fontaine (2013), wave energy E is linearly dependent to the fetch length *x*. Therefore, it can be implied that more wind energy can be transferred to the sea surface for the larger fetch length at FINO 3. One implication of this theory can be seen by the higher average peak wave period (T_p) at FINO 3 compared to FINO 1, with the peak wave periods 7.34 s and 6.98 s respectively.

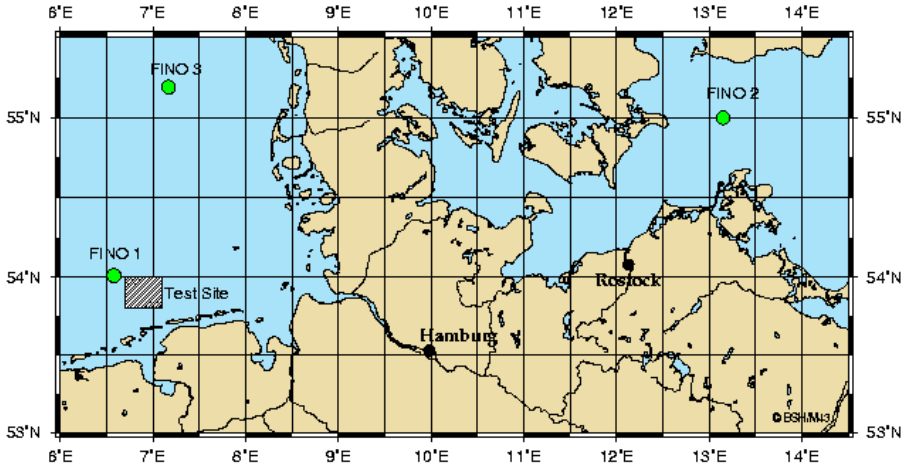

Figure 5.1 Geographic location of FINO 1 and FINO 3 (Bundesamt für Seeschifffahrt und Hydrographie, 2018)

The metocean conditions of interest in this study are wind speed, wind direction, wave direction, significant wave height (Hs), and peak wave period (Tp) at FINO 1 and FINO 3.

Wind and wave rose charts will be presented in the following section in order to understand the metocean conditions at both FINO 1 and FINO 3. The two measurement platforms experience two different environmental exposures in terms of wind and wave type and possible directions. By understanding the metocean conditions, we can discuss why and how the misalignment occurs at certain directions and under certain conditions.

There are three rose charts describing the distribution of wind speeds, magnitude of wave height (Hs), and magnitude of wave period (Tp). A separate rose chart for misalignment was also generated to show the misalignment distribution against wind speed, although the latter does not represent direction in global sense.

5.1.1 FINO 1

The wind speed at 80 m was selected at FINO 1 as this allowed us to select measurements on either side of the mast and avoid distortion effects. This gave the highest data return for the 11 years period analysed in this study (see Section 4.3.1). The existing Alpha Ventus wind farm adjacent to FINO 1 have wind turbines with hub height 90 m. Therefore, corresponding wind direction data at 90 m was used in this study as this was deemed to be the most reliable measurement of wind direction. Moreover, wind direction at 90 m had a high data return (see also Section 4.3.1).

The metocean conditions for FINO 1 are shown below:

1. FINO 1 Wind rose chart
    a. Wind speed distribution along 360 degrees wind direction at 80 m height for 11 years (1st January 2006 00:00 to 1st October 2017 00:00).

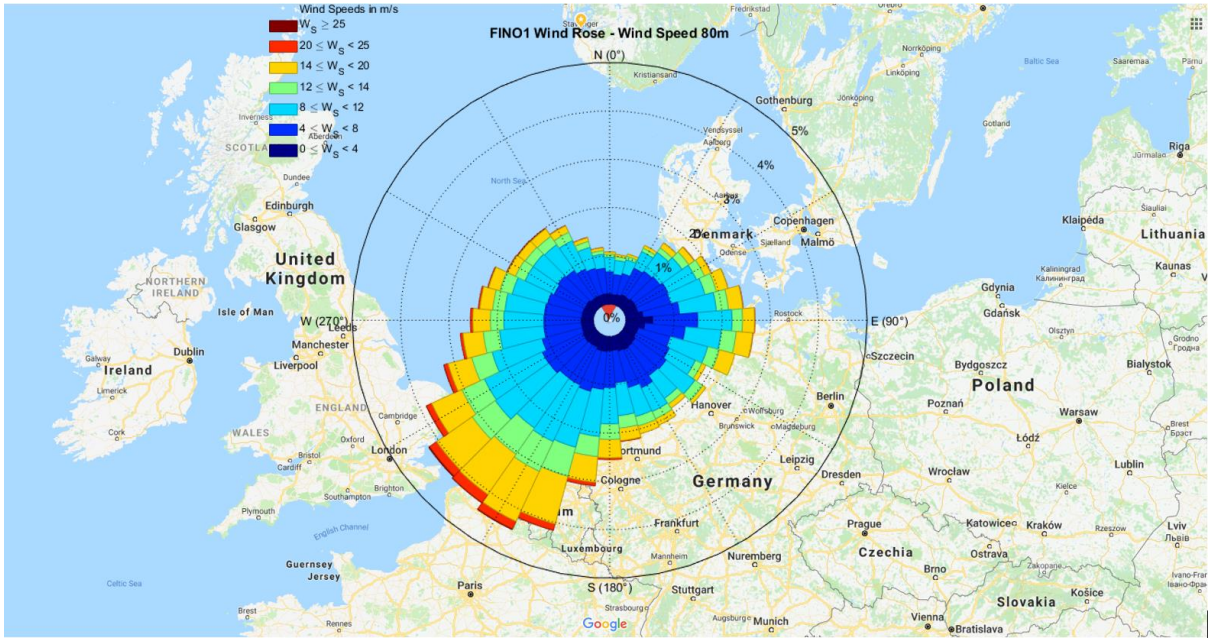

Figure 5.2 Wind rose at FINO 1 for 11 years period with wind speed at 80 m height; alongside google map presentation of FINO 1 location at the North Sea

According to Figure 5.2 above, high wind speeds were coming from the English Channel between France and UK as well as from Belgium side with the highest wind speeds captured

from this South-West (SW) direction in the range of 20 to 25 m/s, and the most frequent wind speeds are in the range of 10 to 15 m/s. The wind speeds distribution in the FINO 1 is consistent with the prediction, that the South-West direction near lands has the higher frequency of high wind speeds because of the land breeze – when winds blow from higher pressure over the land to lower pressure over the sea (Ackerman, 1995). Winds from the North-West (NW) and East direction are the second most frequent with maximum wind speeds between 15 and 20 m/s.

2. FINO 1 Wave rose chart
    a. Significant wave height (Hs) distribution along 360 degrees wave direction for 11 years (1st January 2006 00:00 to 1st October 2017 00:00).

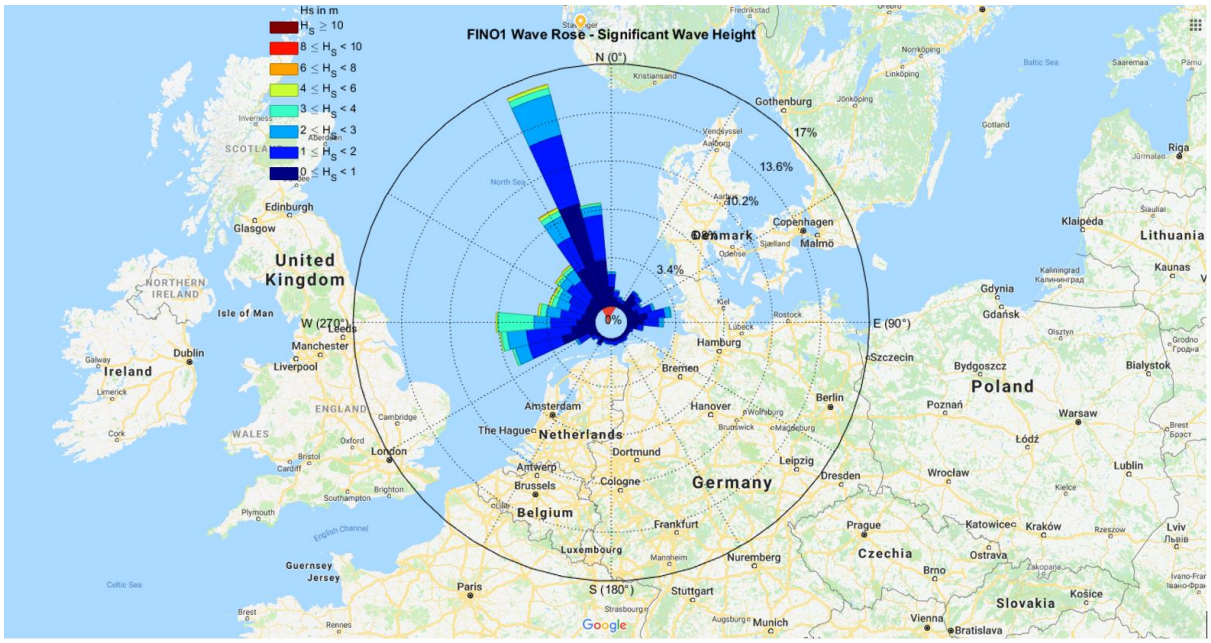

Figure 5.3 Wave rose at FINO 1 for 11 years period with Hs; alongside google map presentation of FINO 1 location at the North Sea.

According to Figure 5.3 above, high significant wave heights were coming from Norwegian Sea near the Iceland and Greenland area with the highest Hs captured from this North-North-West (NNW) direction are in the range of 5 to 8 m, while very high Hs above 8 m were scarce. This highest Hs coming from NNW direction is directly related to waves being created by distant storms in the Barents Sea, which is apparent by the long fetch distance from the north of the FINO 1 location. The second most frequent Hs with medium range heights are coming from the West-South-West (WSW) direction with maximum Hs between 2 and 5 m. On the other hand, frequency and magnitude of Hs captured from North-East and South directions are very low.

b. Peak Wave Period (Tp) distribution along 360 degrees wave direction for 11 years (1st January 2006 00:00 to 1st October 2017 00:00).

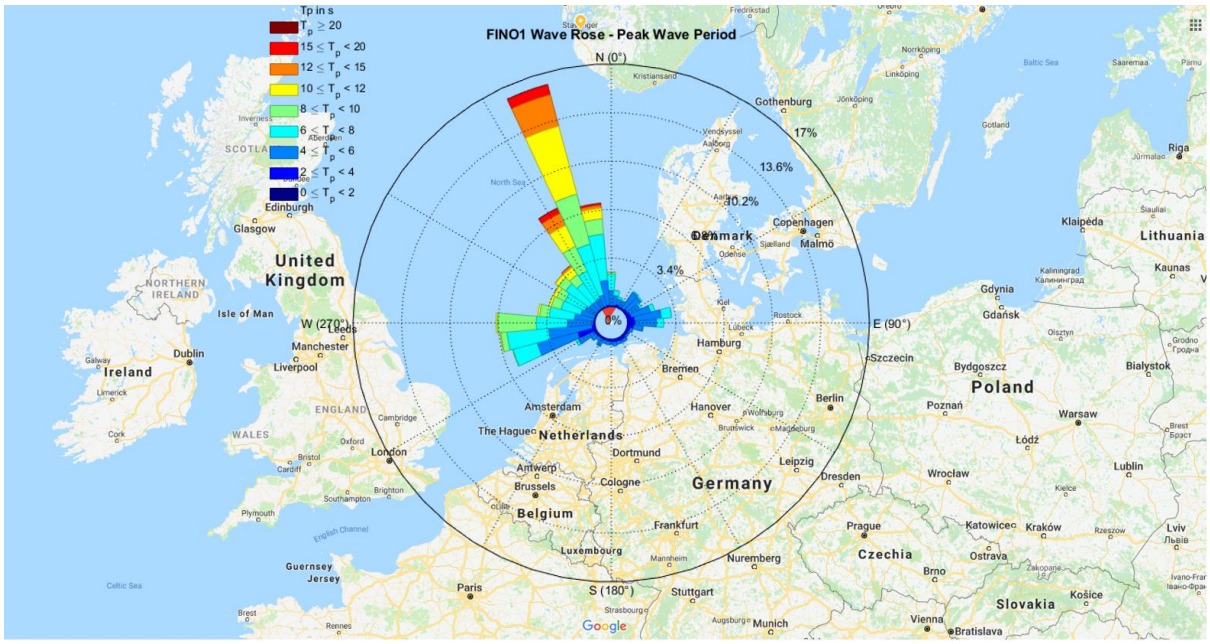

Figure 5.4 Wave rose at FINO 1 for 11 years period with Tp; alongside google map presentation of FINO 1 location at the North Sea.

Waves with peak wave period more than 10 s are assumed to be swell which in this case resembles the direction in a sensible way. According to Figure 5.4 above, the long fetch in the North Sea between UK and Norway (waves coming from Norwegian Sea) allows swell to propagate and carry high energy waves towards FINO 1. The highest wave periods were observed from this North-North-West (NNW) direction and are in the range of 15 to 20 s, while very high Tp above 20 m were scarce. The second most frequent Tp wave direction is coming from the West-South-West (WSW) direction with peak periods no more than 10 s. The frequency and magnitude of Tp captured from North-East and South directions are very low as expected due to shorter fetch length.

5.1.2 FINO 3

In contrast to FINO 1, the FINO 3 measurement mast was redesigned with the triangular base mast shape to reduce distortion effects. Therefore, the wind speeds and wind directions used at FINO 3 were both at 90 m height.

The metocean conditions for FINO 3 are shown below:

1. FINO 3 Wind rose chart
    a. Wind speed distribution along 360 degrees wind direction at 90 m height for 8 years (1st October 2009 00:00 to 2st October 2017 00:00).

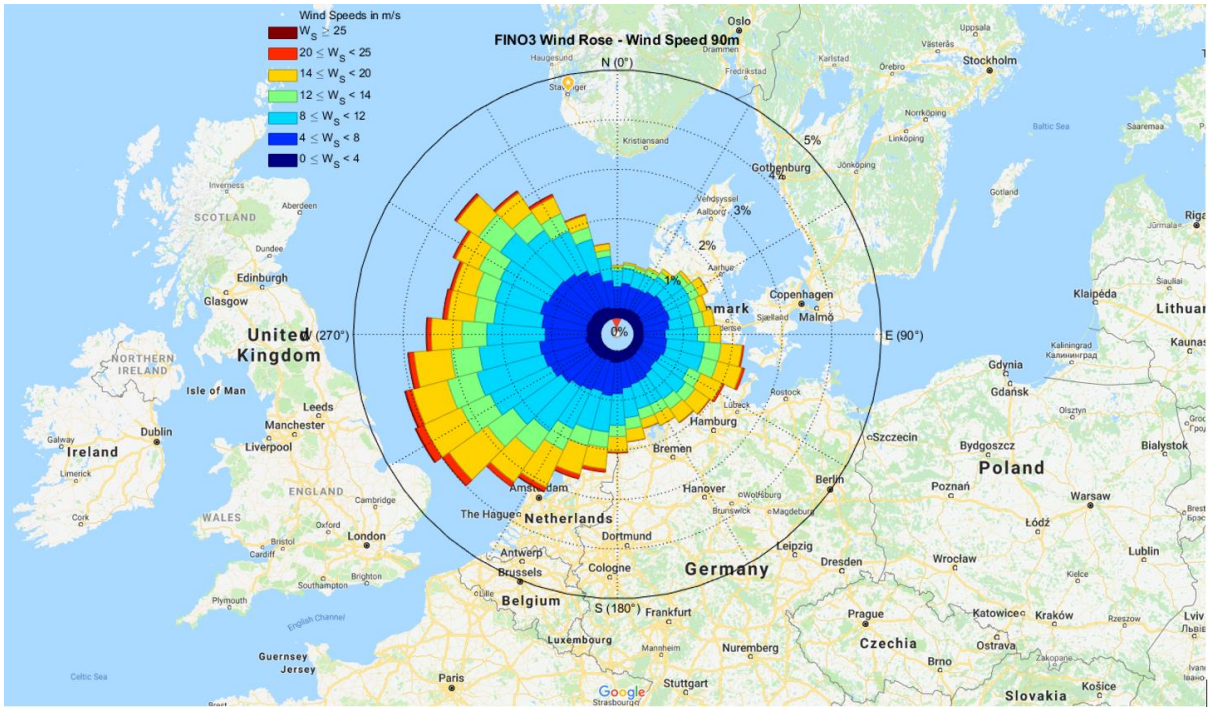

Figure 5.5 Wind rose at FINO 3 for 8 years period with wind speed at 92 m height; alongside google map presentation of FINO 3 location at the North Sea.

According to Figure 5.5 above, the prevailing high wind speeds are in westerly direction, found to be higher at South-West direction which is similar to FINO 1 but having a higher frequency of moderate wind speeds from the North-West direction. The highest wind speeds captured from the South-West direction are in the range of 20 to 25 m/s, whereas the most frequent wind speeds occur in the range of 10 to 15 m/s. Wind speeds distribution in the FINO 3 wind rose is looking more spread throughout the westerly directions, which could be due its more northerly location. Whereas the east direction is the second most frequent with maximum wind speeds between 15 and 20 m/s.

2. FINO 3 Wave rose chart
    a. Significant wave height (Hs) distribution along 360 degrees wave direction for 8 years (1st October 2009 00:00 to 2nd October 2017 00:00).

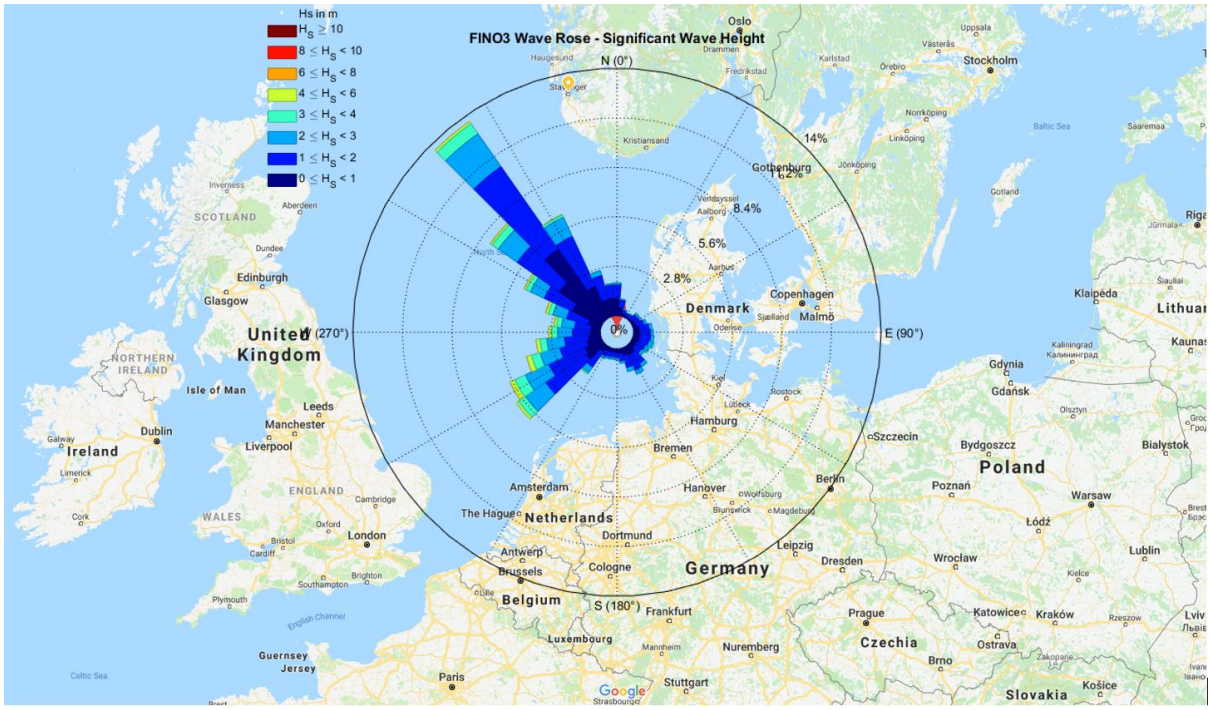

Figure 5.6 Wave rose at FINO 3 for 8 years period with Hs; alongside google map presentation of FINO 1 location at the North Sea.

As shown in Figure 5.6 above, the largest significant wave heights were observed coming from Norwegian Sea near the Iceland and Greenland area. The highest Hs captured from this North-North-West (NNW) direction and was in the range of 5 to 8 m, while very high Hs above 8 m were scarce. Similar to the results observed at FINO 1, the larger wave heights from the north are most likely due to storm system in the Northern North Sea area. However, the secondary peak in wave height which comes from the West-South-West (WSW) direction with maximum Hs between 6 and 7 m are the result of a long fetch length and prevailing south westerly winds. Similar to the previous results from FINO 1, the frequency and magnitude of Hs captured from East and South directions are very low.

b. Peak Wave Period (Tp) distribution along 360 degrees wave direction for 8 years (1st October 2009 00:00 to 2st October 2017 00:00).

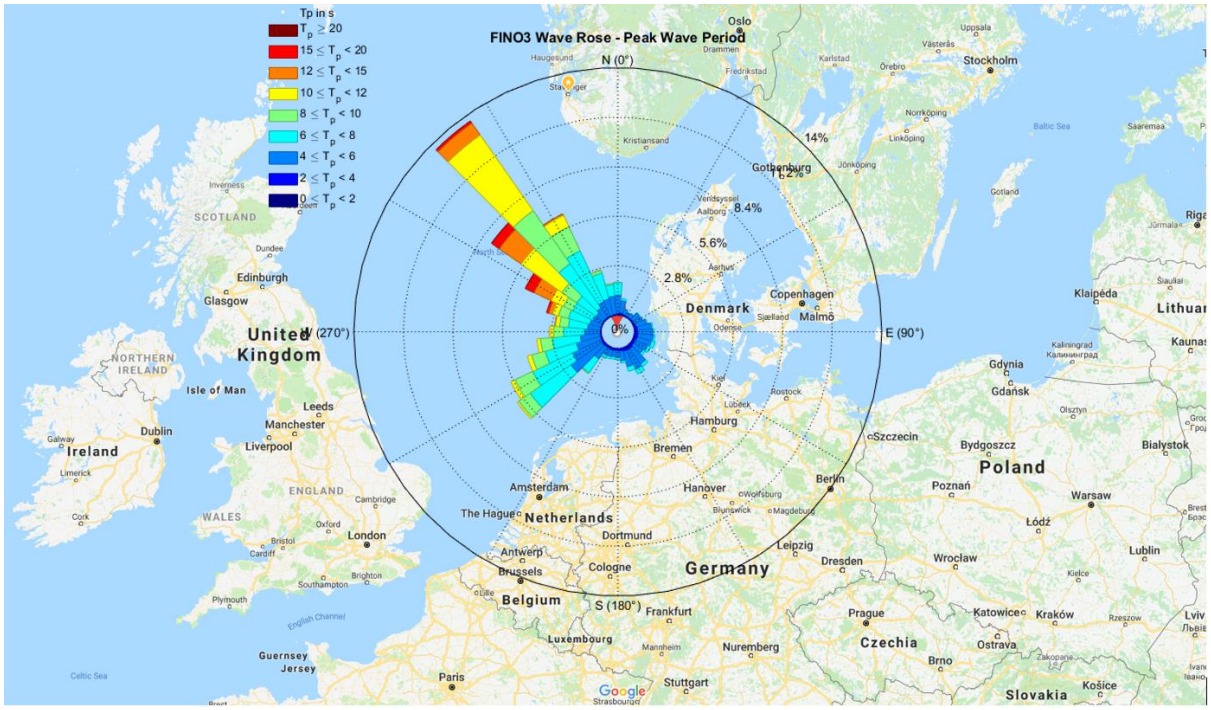

Figure 5.7. Wave rose for 2 years FINO 3 data - Tp - including North Sea map centered at FINO 3

As explained previously, the long fetch in the North Sea between UK and Norway (waves coming from Norwegian Sea) allows swell to propagate and carry high energy waves towards FINO 3 as well. This is more apparent at FINO 3 where the highest wave periods are observed coming from the North-West (NW) direction are in the range of 15 to 20 s, while very high Tp above 20 m were scarce. The secondary peak in Tp occurs in West-South-West (WSW) direction with peak period no more than 10 s. On the other hand, frequency and magnitude of Tp captured from North-East and South directions are very low as expected given the shorter fetch length.

5.2 Wind-wave misalignment frequency of occurrence

Wind-wave misalignment frequency of occurrence is calculated by the method described in Chapter 4.4. At FINO 1 and FINO 3 the wind direction data at 90 m are used and both buoy wave direction is used for this assessment. To calculate the wind-wave misalignment, wave direction is subtracted from the wind direction with the aim of obtaining the smaller acute angle of the misalignment, when considering the direction value passing the 360 degrees mark.

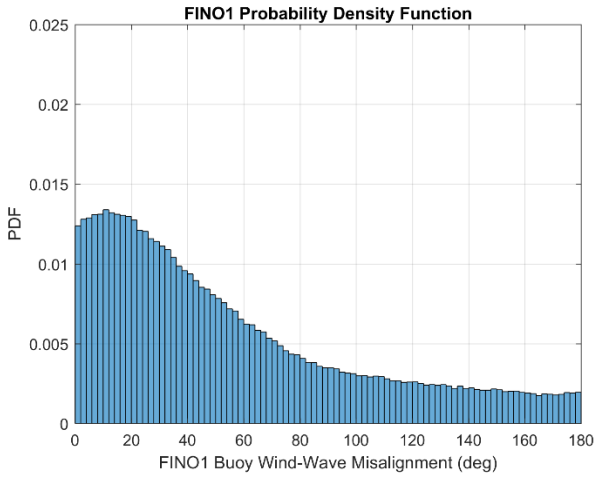

Figure 5.8 FINO 1 probability density function of wind-wave misalignment for 11 years period.

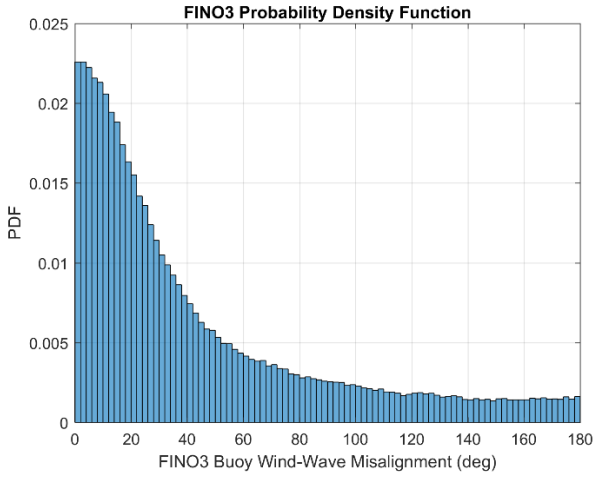

Figure 5.9 FINO 1 probability density function of wind-wave misalignment for 8 years period.

The probability density function of the wind-wave misalignment considering the absolute values of the misalignments is presented in Figure 5.8 and Figure 5.9 above for FINO 1 and FINO 3 respectively. The figures show that the probability of occurrence decreases with increasing wind-wave misalignment. Where 0-degree represents complete alignment and 180-degree complete misalignment (opposite). The PDF chart above shows that the probability distribution is narrower for the FINO 3 compared to FINO 1, indicating that aligned wind and wave occurs a higher percentage of the time.

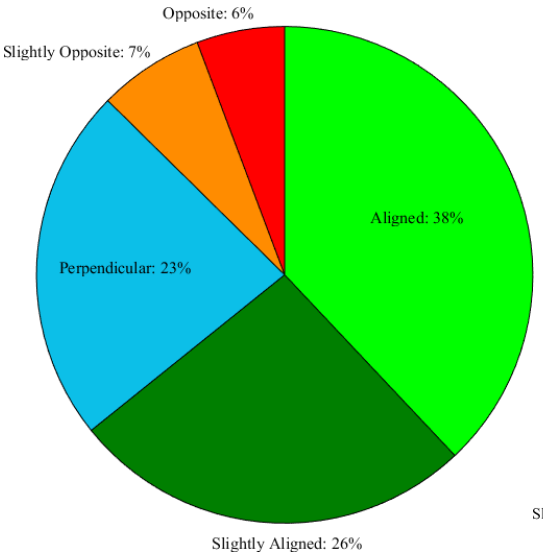

Figure 5.10 FINO 1 Wind-wave misalignment frequency of 11 years data.

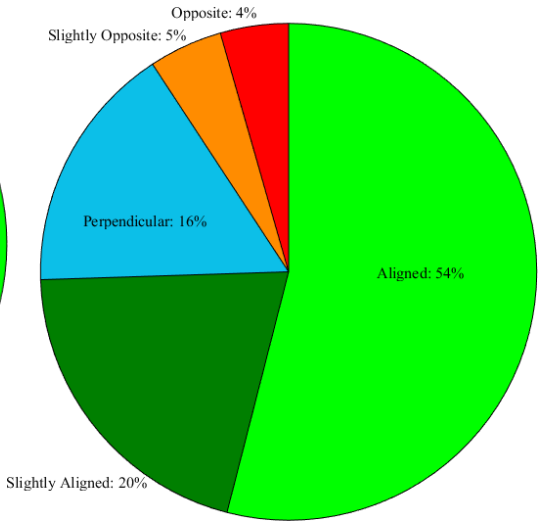

Figure 5.11 FINO 3 Wind-wave misalignment frequency of 8 years data.

In a categorized way, Figure 5.10 and Figure 5.11 present the wind wave misalignment frequency of occurrence, according to the magnitude of misalignment as defined in Chapter 3.3.

Wind-wave misalignments occurrence for each platform shows that total misalignment higher than 60° is 36% at FINO 1 and 25% at FINO 3. Furthermore, the percentage of aligned wind and waves less than 30° misalignment is higher at FINO 3 compared to FINO 1 by 54% to 38 % respectively. Looking at the results, there was a slightly higher percentage of misaligned wind wave conditions at FINO 1, but the general pattern is similar at both sites. In particular, opposing wind-wave misalignment, which suggest misalignment above 120°, is infrequent, with 13% occurrence at FINO 1 and 9% occurrence at FINO 3. The interesting point of these results is that a significant number of perpendicular wind wave conditions was observed at FINO 1 and FINO 3 (23% and 16% respectively) which could influence both the power production and loading of an offshore wind turbine, as the assumption in the design process is that the wind and waves are aligned.

A similar investigation on wind-wave misalignment in the Dutch North Sea site by Kühn (2001) shows similar findings that misalignment up to 30° is common, while misalignment larger than 60° occurs less than 5% of the time, as shown in Figure 3.3. Numerical simulations by Kühn (2001) showed the hydrodynamic fatigue response of a fixed monopile offshore wind turbine, Kühn (2001) stated that when the above misalignment of the mean wind and wave direction is taken into account, observation shows that the aerodynamic response in lateral direction is more than double compared to the collinear wind-wave condition. Particularly,

there were notable changes of the distribution of the damage equivalent stress range in wind turbine monopile up to misalignment 30°. Whereas for large misalignments of 60° and 90°, the absence of aerodynamic damping increases the wave response and it exceeds the maximum total loading for collinear conditions.

5.3 Wind-wave misalignment frequency under swell and wind-wave

Statistical analysis done by Semedo et al. (2011) shows that the global ocean wave field is dominated mainly by swell waves, characterized by longer periods wave. Although it should be noted that swell waves have different natures and different impacts on the MABL and ocean mixing layer, depending on the age and distance to the generating storm.

In this study swell wave conditions are assumed to be peak wave periods greater than 10 s. Wind-wave misalignment frequency relative to the observed wave condition (i.e. swell or wind wave condition) is shown in Figure 5.12 and Figure 5.13 below. The hatched areas show the portions of misalignment under swell wave (Tp above 10 s), whereas the solid area shows the misalignment under wind wave (Tp below 10 s). The percentages showing in the pie chart are the portions of certain misalignment conditions relative to the whole respective data set, 11 years period for FINO 1 and 8 years period for FINO 3. To be noted that the empty tiny sector shown at FINO 3 pie chart is due to the fact that 1% the wave period data was not available for this location.

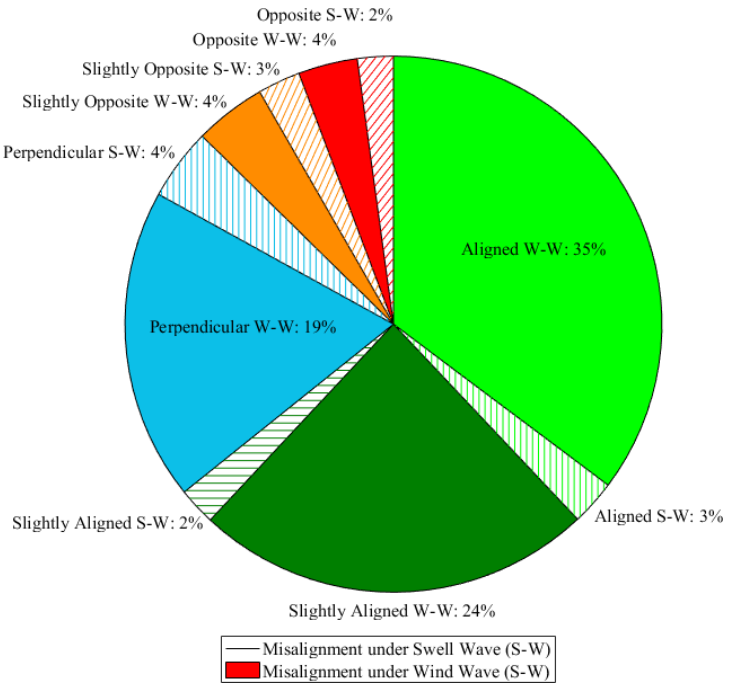

Figure 5.12. FINO 1 Swell-Wind Wave misalignment frequency of 11 years data

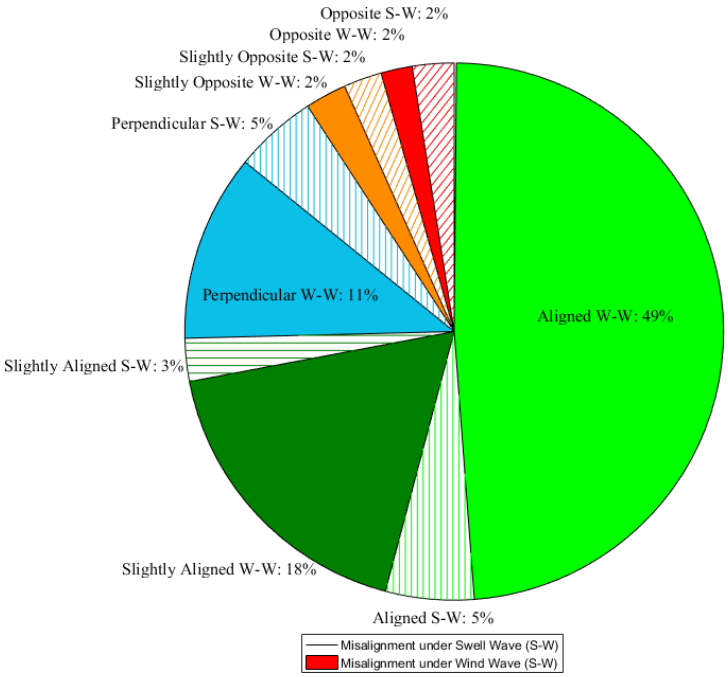

Figure 5.13. FINO 3 Swell-Wind Wave misalignment frequency of 8 years data

In general, the above charts show that the misalignment under swell is considerably lower than the misalignment under wind wave conditions. 14% of the wind-wave misalignment observed at FINO 1 and 17% at FINO 3 were occurring under swell wave system. As expected, the ratio of misalignment under swell wave increases with the increase in misalignment magnitude. For FINO 1, Opposing misalignment consists of 5 percent under swell wave, with the population of opposing misalignment occurrence at 13 percent, that leads to nearly 0.4 ratio of opposing misalignment under swell wave system. In contrast, the ratio of aligned wind-wave under swell wave is less than 0.1 (5 percent aligned under S-W out of 64 percent total aligned). Meanwhile, for perpendicular misalignment, the ratio is approximately 0.2. It can be seen that a significant portion of opposing misalignment occurred under swell wave, which is expected as the high period wave carrying high energy can result in wave induced wind.

Previous CFD simulations by Sullivan et al (2008) suggested that wind wave misalignment (opposing) under swell conditions could have a significant effect on turbulent wind loads on a wind turbine. Vertical profiles of wind velocity and turbulent kinetic energy show distinct differences for waves aligned with the wind versus waves opposing the wind. A speed-up near the wave surface is present when the wind is aligned with a faster moving wave surface. In contrast, a notable effect was observed when the wave is opposing the wind. When the wave is opposing the wind, the wind velocity will be reduced in the lower heights and occasionally reverted.

However, our results suggest that opposing misalignment under swell conditions is not a common condition in the North Sea.

5.4 Wind speed distribution when wind-wave misaligned

The wind speed distribution when the wind-waves are misaligned is important to determine the relative importance for power production and loading of an offshore wind turbine. A simple histogram is used to present the distribution of wind speed according to the misalignment conditions at FINO 1 and FINO 3. Figure 5.14 to Figure 5.18 show results from FINO 1 and Figure 5.19 to Figure 5.23 show results from FINO 3. In general, the results from FINO 1 and FINO 3 have similar patterns. One difference is that the global mean (mean wind speed in total) is higher in FINO 3. As expected the mean wind speed when the wind and waves are aligned is higher than when the wind and waves are misaligned. For FINO 1, the mean wind speed is 10.2 m/s for aligned condition and 7.7 m/s for misaligned condition as shown in Figure 5.14 and Figure 5.15. Whereas for FINO 3, the mean wind speed is 10.7 m/s for aligned condition and 7 m/s for misaligned condition as shown in Figure 5.14 and Figure 5.15. Looking at Figure 5.16 when perpendicular misalignment occurs in FINO 1, there is a considerably lower mean wind speed observed, compared to aligned condition, the decrease from 10.2 m/s to 8.3 m/s can be a big impact in power production of offshore wind turbine in a long run. The same situation applies for FINO 3 with even higher difference, where the mean wind speed decreases from 10.7 m/s under aligned condition to 7.3 m/s under perpendicular condition.

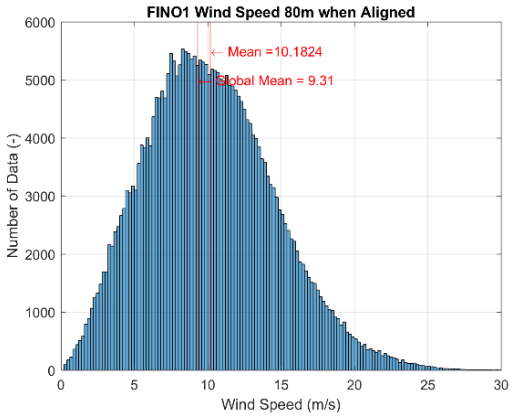

Figure 5.14. FINO 1 Wind Speed Histogram – Total Aligned

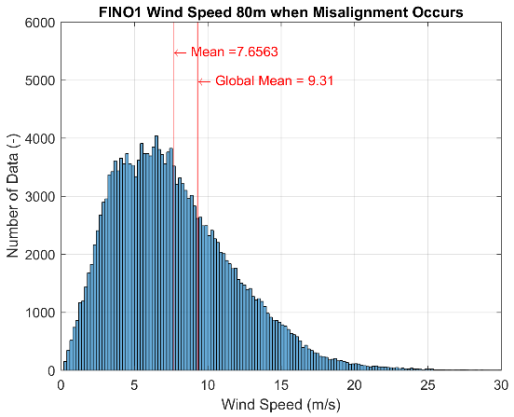

Figure 5.15. FINO 1 Wind Speed Histogram – Total Misaligned

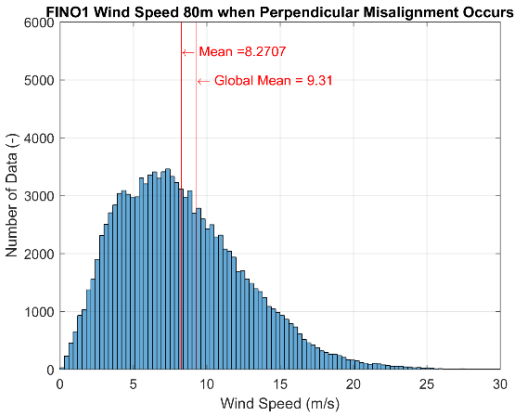

Figure 5.16 FINO 1 Wind Speed Histogram – Perpendicular Misaligned

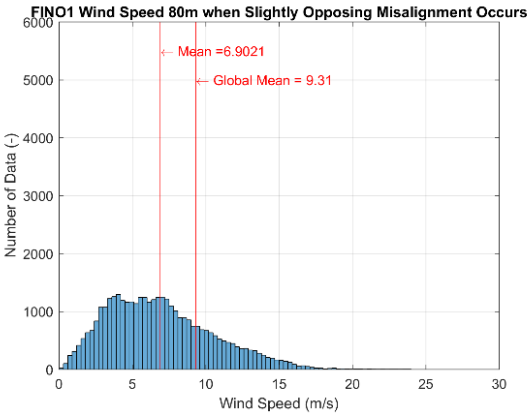

Figure 5.17 FINO 1 Wind Speed Histogram – Opposing Misaligned

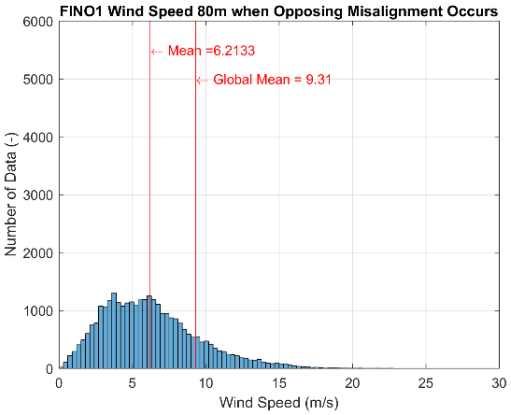

Figure 5.18. FINO 1 Wind Speed Histogram – Opposing Misaligned

Offshore wind turbines are only operational for wind speeds greater than 5 m/s. Figure 5.17 and Figure 5.18 for FINO 1 as well as Figure 5.22 and Figure 5.23 for FINO 3 shows that for the condition of wind opposing waves there were observed only a small percentage of conditions which occur in the range of wind speeds relevant for an offshore wind turbine (7% and 4% for FINO 1 and FINO 3 respectively). Figure 5.16 and Figure 5.22 however do show that a significant number of conditions occur at moderate and higher wind speeds when the wind and waves are perpendicular.

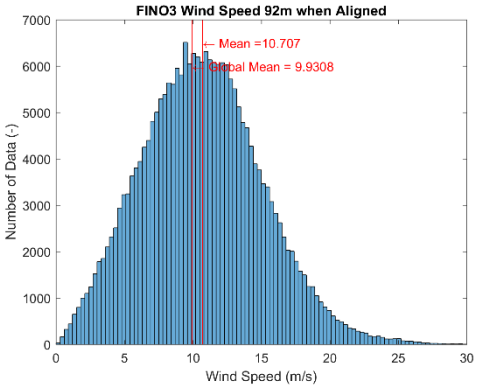

Figure 5.19 FINO 3 Wind Speed Histogram – Total Aligned

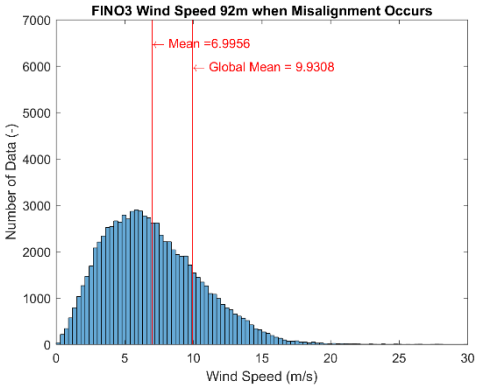

Figure 5.20. FINO 3 Wind Speed Histogram – Total Misaligned

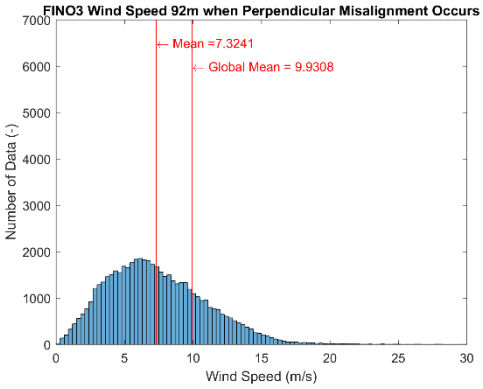

Figure 5.21 FINO 3 Wind Speed Histogram – Slightly Opposing Misaligned

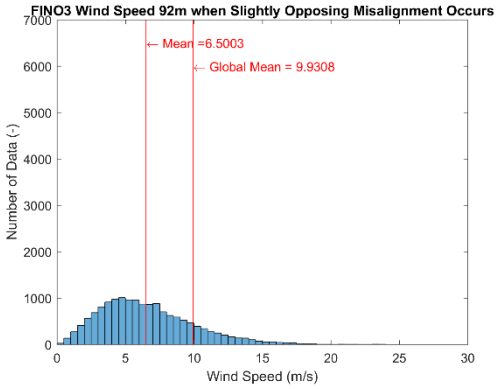

Figure 5.22 FINO 3 Wind Speed Histogram – Total Perpendicular Misaligned

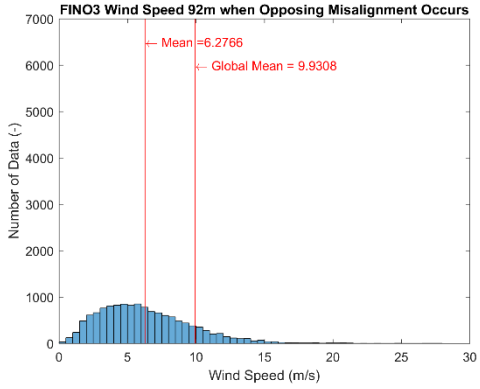

Figure 5.23 FINO 3 Wind Speed Histogram – Total Opposing Misaligned

Bachynski et al. (2014) investigated using numerical simulations a certain selection of misaligned wind and wave conditions. The study found increased motions of an offshore wind turbine for both parallel and perpendicular wind-wave misalignment. However, aligned wind and waves caused the largest short-term tower base fatigue damage for the studied platforms

and conditions. Our results suggest that simulations when the wind and wave are perpendicular to each other should be investigated further in relation to the design of offshore wind turbines.

The misalignment rose diagrams are shown in Figure 5.24 and Figure 5.25 to further visualize the distribution of wind speed under different misalignment conditions. It is important to note that in the following figures the angles represent the level of misalignment between the wind and waves, not the geographic direction.

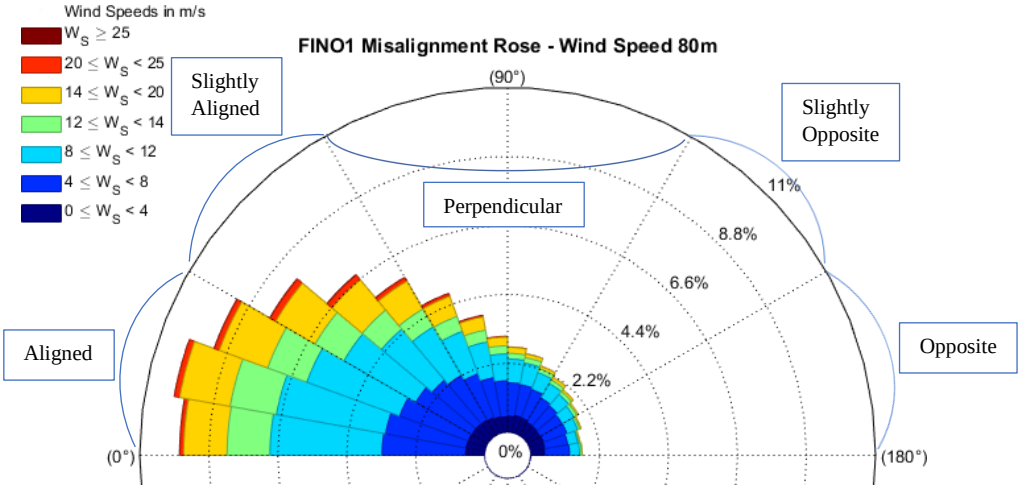

Figure 5.24 FINO 1 Misalignment Rose

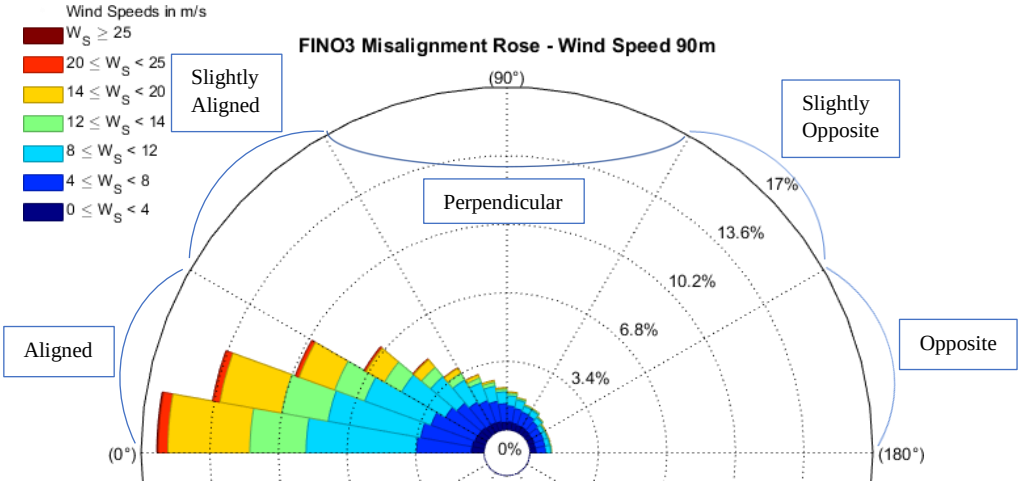

Figure 5.25 FINO 3 Misalignment Rose

At both platforms, the dominant wind speeds occur between 10° and 20° misalignment (10% of the time), whereas 0° up to 10° misalignment occurs no more than 10% at which less frequent. However, in general, from the two figures above, it is shown that the mean wind speed reduces with the increment in wind-wave misalignment as expected. The misalignment rose shows that a large range of wind speeds occur for all levels of wind wave misalignment, but the frequency of occurrence reduces. However, the highest wind speeds were typically

observed under aligned and slightly aligned conditions as expected. Some high wind speeds were observed for a misalignment of 70-80° and this could well be due to high winds veering in storm condition, but further investigation is necessary to confirm this. In a growing sea state, the wind and waves will often be initially misaligned but after a certain length of time, wind and wave start to align (WMO, 1998) and this could account for the high level of observed perpendicular wind wave misalignment conditions.

5.5 Turbulence intensity

Turbulence intensities at several heights are presented from the OBLEX data set (15 and 20 m) and FINO dataset (30 and 40 m). The ratio of standard deviation over mean wind speed at certain height was calculated for each data points to plot the turbulence intensity chart, as described in Chapter 2.5.1.

The data for turbulence intensity plots were selected from wind directions 30° to 240°, since these directions were deemed to be the undisturbed wind speed sector for the 15 m and 20 m sonic anemometers at FINO 1.

In terms of turbulence intensity, the interests in this thesis are to look into the turbulence intensity according to the wind-wave misalignment conditions. Overall turbulence intensity plotted as a scatter chart with distinct colour for each misalignment classification at 30 m and 40 m height are shown in Figure 5.26 and Figure 5.27 respectively. In general, the long-term data shows that the opposite misalignment condition has the tendency of having lowest turbulence intensity, and are clustered around lower wind speeds.

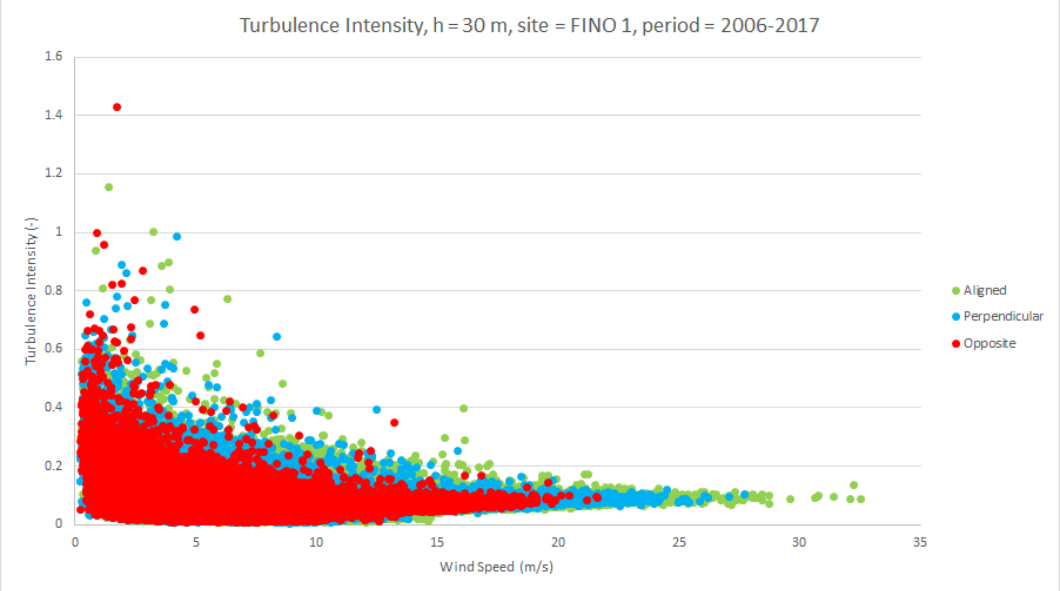

Figure 5.26 FINO 1 Turbulence intensity at 30 m height across the 11 years period.

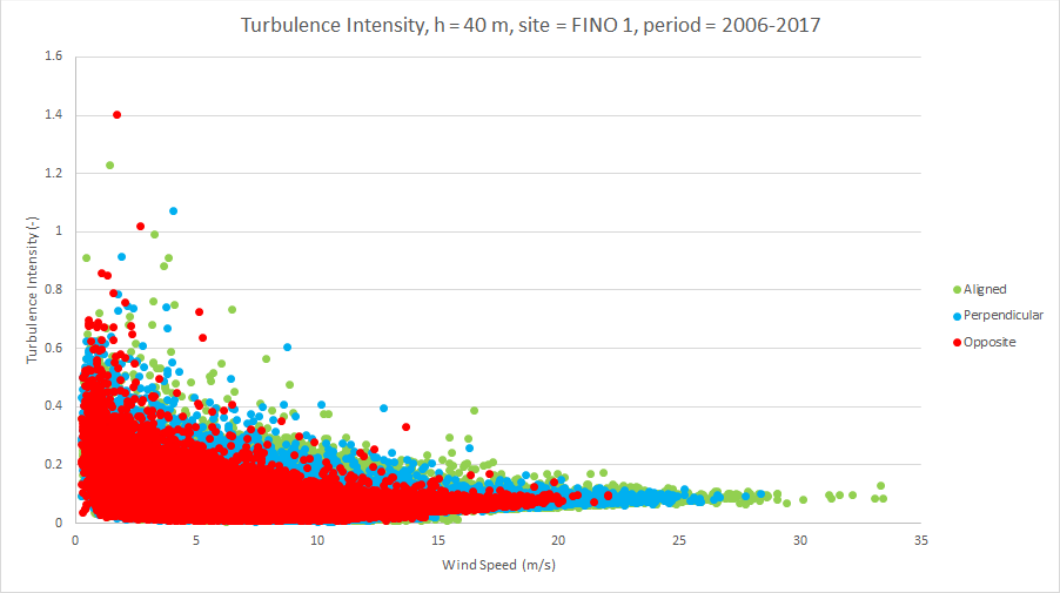

Figure 5.27 FINO 1 Turbulence intensity at 40 m height across the 11 years period.

The bin average plots presented in Figure 5.28 and Figure 5.29 below provides a clearer depiction of the moving average comparison between each misalignment condition.

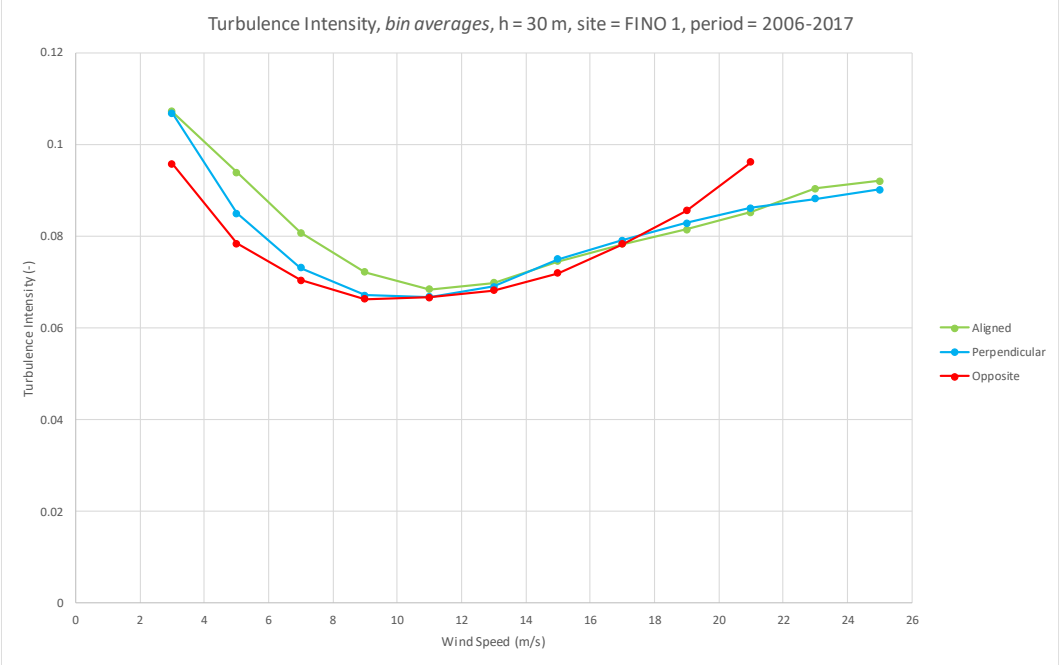

Figure 5.28 FINO 1 Turbulence intensity bin averages at 30 m height across the 11 years period.

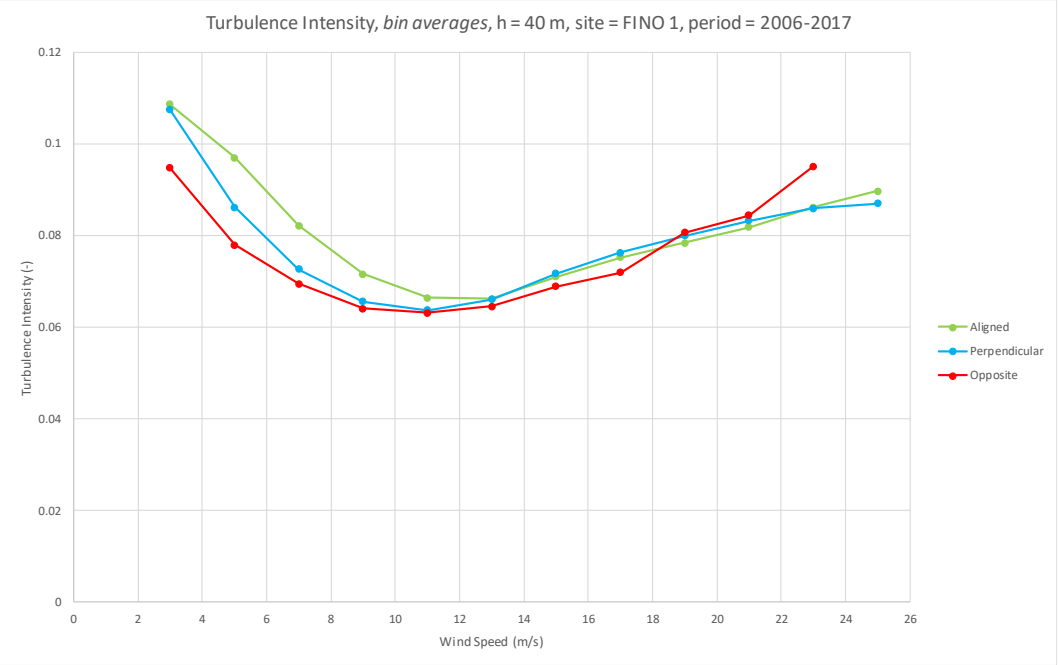

Figure 5.29 FINO 1 Turbulence intensity bin averages at 40 m height across the 11 years period.

The bin average plots of turbulence intensity above show in general, that there is a similar pattern, at both 30m and 40m, having a minimum turbulence intensity (TI) found at around 11 m/s for both sites, and an increase of turbulence intensity above 11 m/s. The produced bin average plots were in agreement to a research by Westerhellweg et al. (2010) as referenced in Figure 3.4. An interesting point to see is that there is an increase beyond the wind speed 18 m/s where the TI of the opposite misalignment become the highest, although this could be attributed to the less occurrence of high wind speed in opposing condition.

The results at 30 m and 40 m heights are similar in that they both show that lower turbulence intensities were observed when the wind was opposing the waves. LES simulations performed by Sullivan et al (2008) found that when light winds oppose the propagating swell, turbulence levels increase over the depth of the boundary layer and the surface drag increases by a factor of 4 compared to a flat surface. This is contrary to the results shown in this study, therefore a further analysis in this thesis has been conducted to observe the cause of this difference.

A previous study by Kalvig (2014) used CFD simulations to demonstrate the effect wind wave misalignment has on a fixed offshore wind turbine. They found that the waves influence the wind field far up into the marine atmospheric boundary layer and this depends on the wave state and the direction of the waves and the wind. Structural simulations in FAST also demonstrated that swell could potentially increase the fatigue damage compared to a situation with no waves, especially for the cases where the wave field opposes the wind field.

Observations from the FINO 1 platform at 30m and 40 m do not however seem to show enhanced levels of turbulence for the situation of wind opposing waves. Due to lower surface roughness the surface layer height offshore can be as low as 30 to 40 m especially under stable conditions (Gryning et al., 2007). It would therefore be interesting to see if we can observe enhanced turbulence for opposing conditions at lower levels closer to the water surface.

For the observed conditions of wind opposing waves, the average wave period at FINO 1 was 8.7 s, and the average wave height was 1.1 m. The average wave height under aligned and misaligned wind wave conditions was 1.6 m and 1.23 m respectively. A study by (Westerhellweg et al., 2010) conclude that the wave height and the atmospheric stability are two driven factors of the range of turbulence intensities at FINO 1 and FINO 3. Therefore, bin average plot on wind speed against significant wave height (Hs), and wind speed against peak wave period (Tp) were produced in Figure 5.30 and Figure 5.31 below. The wind speeds in the range of 3 m/s to 15 m/s were selected considering the data reliability.

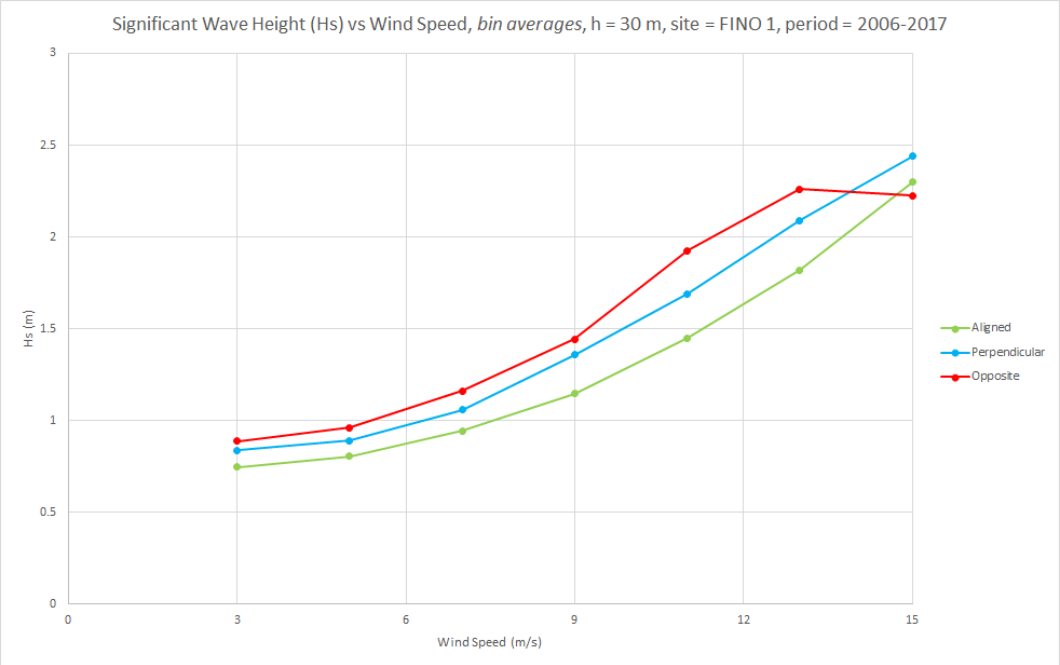

Figure 5.30 Hs vs wind speed bin averages at 30 m height across 11 years period.

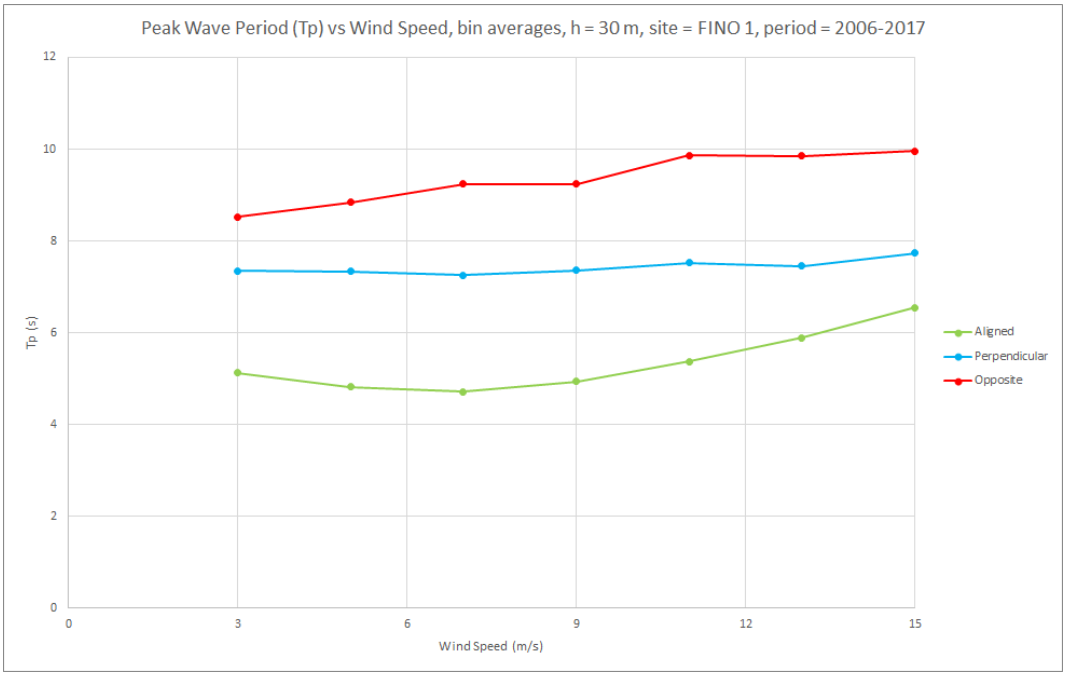

Figure 5.31 Tp vs wind speed bin averages at 30 m height across 11 years period.

Figure 5.30 shows that along the wind speed 3 m/s to 15 m/s, the significant wave heights (Hs) was observed to be the highest for opposing misalignment, although the difference of Hs between the three misalignment conditions were not significant. The Hs values increasing with wind speeds has confirmed the previous findings that the wind wave system is more frequent as expected. On the other hand, along the same wind speed ranges, Figure 5.31 shows that higher peak wave periods (Tp) also found for opposing misalignment. However, the results suggest the wave heights does not seem to result in a high surface roughness that could explain the observed lower intensities found at opposing misalignment.

Moreover, lower heights turbulence intensities generated from the OBLEX data at 15 m and 20 m was produced to see whether there is an enhanced turbulence intensity for opposing misalignment at these lower heights. To be noted that the period of OBLEX data is one month, stretching from 15 September 2015 to 15 October 2015. The turbulence intensity at the corresponding period for the 30 m and 40 m height at FINO 1 are also presented as below.

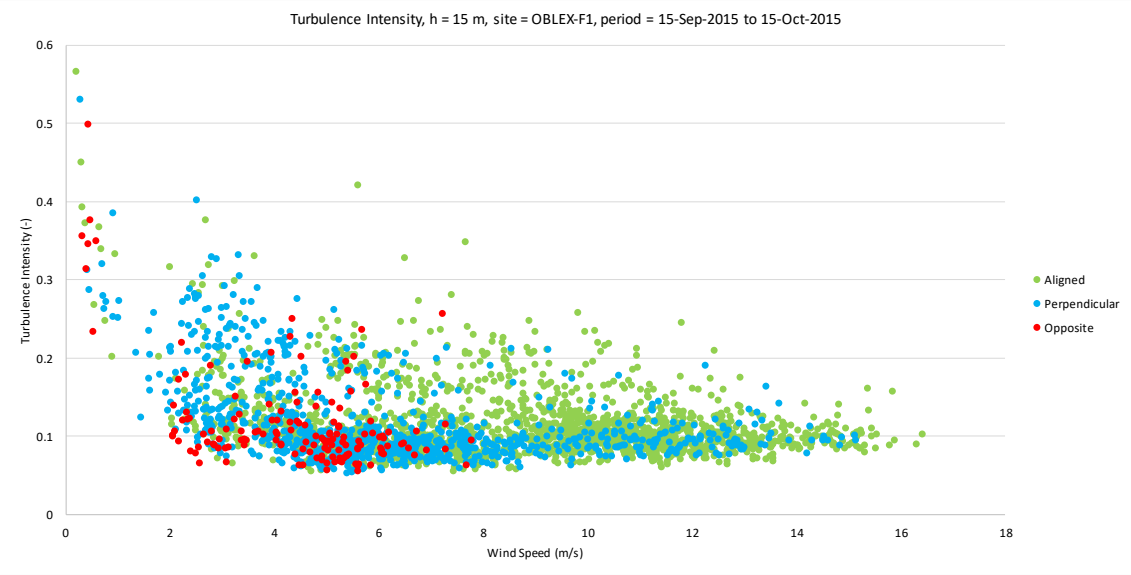

Figure 5.32 OBLEX-F1 Turbulence intensity at 15 m height for 1-month period.

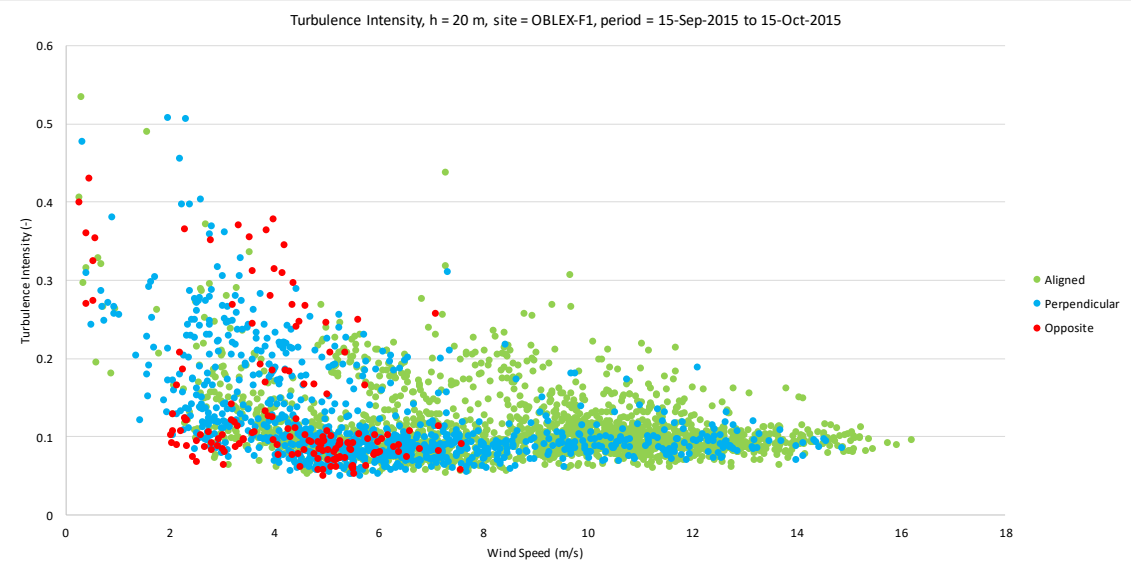

Figure 5.33 OBLEX-F1 Turbulence intensity at 20 m height for 1-month period.

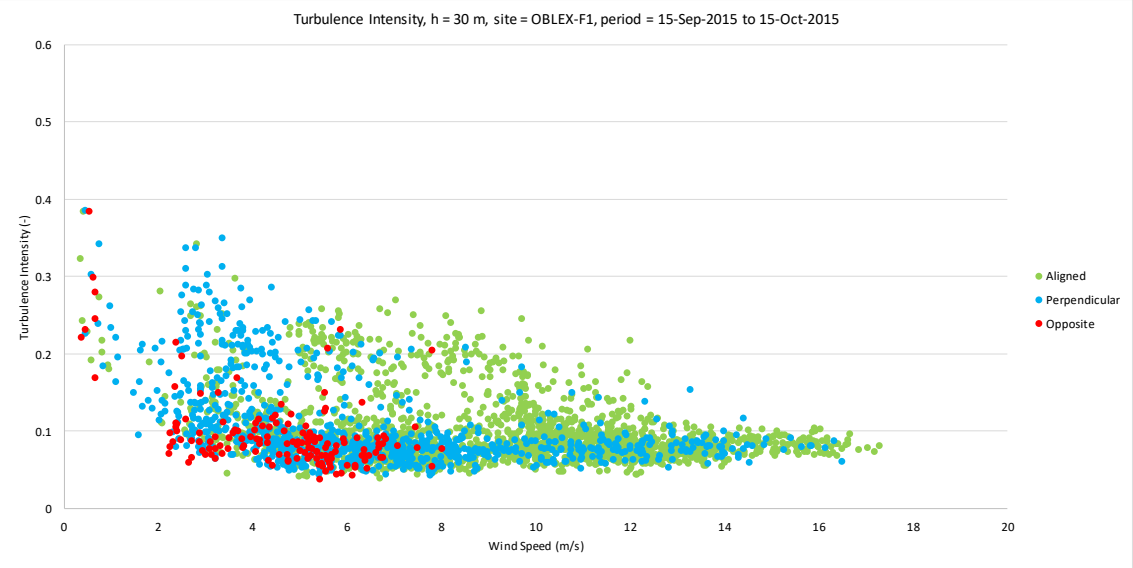

Figure 5.34 OBLEX-F1 Turbulence intensity at 30 m height for 1-month period.

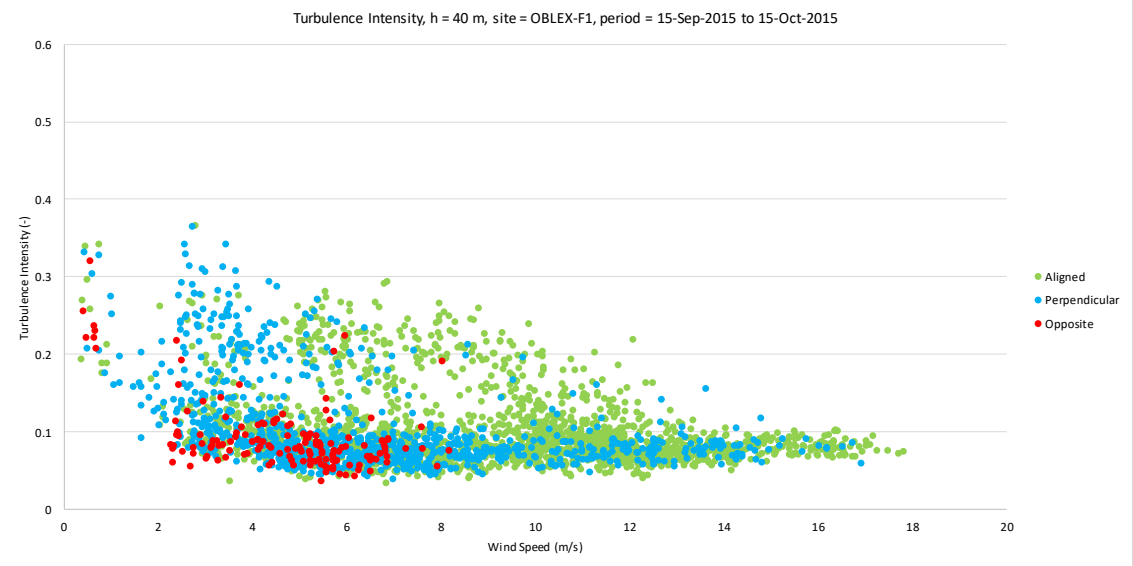

Figure 5.35 OBLEX-F1 Turbulence intensity at 40 m height for 1-month period.

As shown in Figure 5.32 and Figure 5.33, the similar pattern can be observed with lower turbulence intensities observed at 15 m and 20 m heights when the wind was opposing the waves. In the 1-month period, there is no wind speed for opposing condition observed higher than 8 m/s. Similar conditions can be seen at the higher heights at 30 m and 40 m, see Figure 5.34 and Figure 5.35.

In order to see the comparison between each misalignment classification, bin averages plot was produced in Figure 5.36 to Figure 5.39 below.

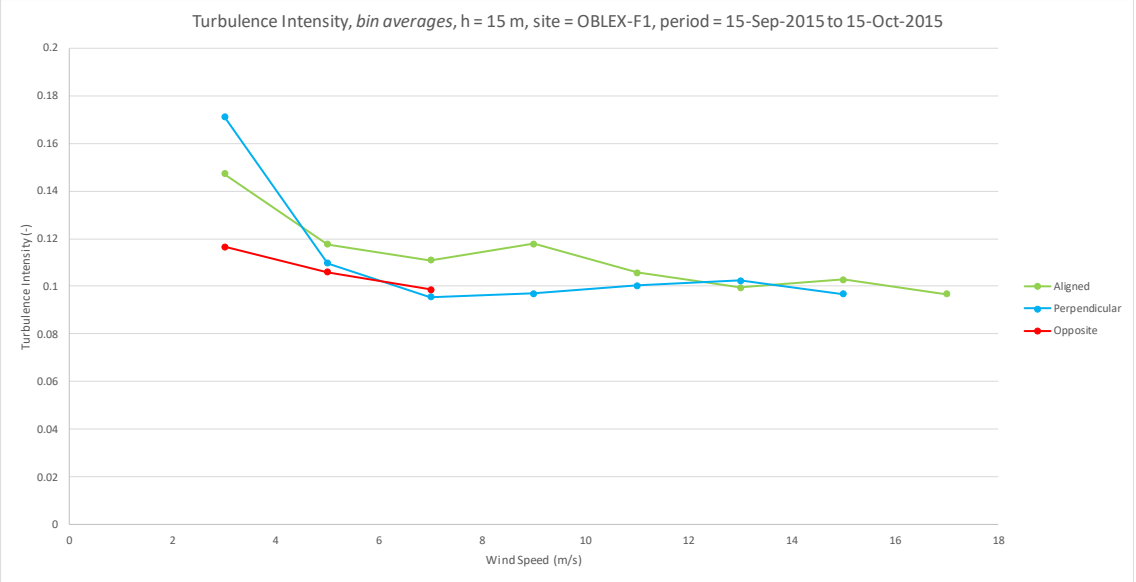

Figure 5.36 OBLEX-F1 Turbulence intensity bin averages at 15 m height for 1-month period.

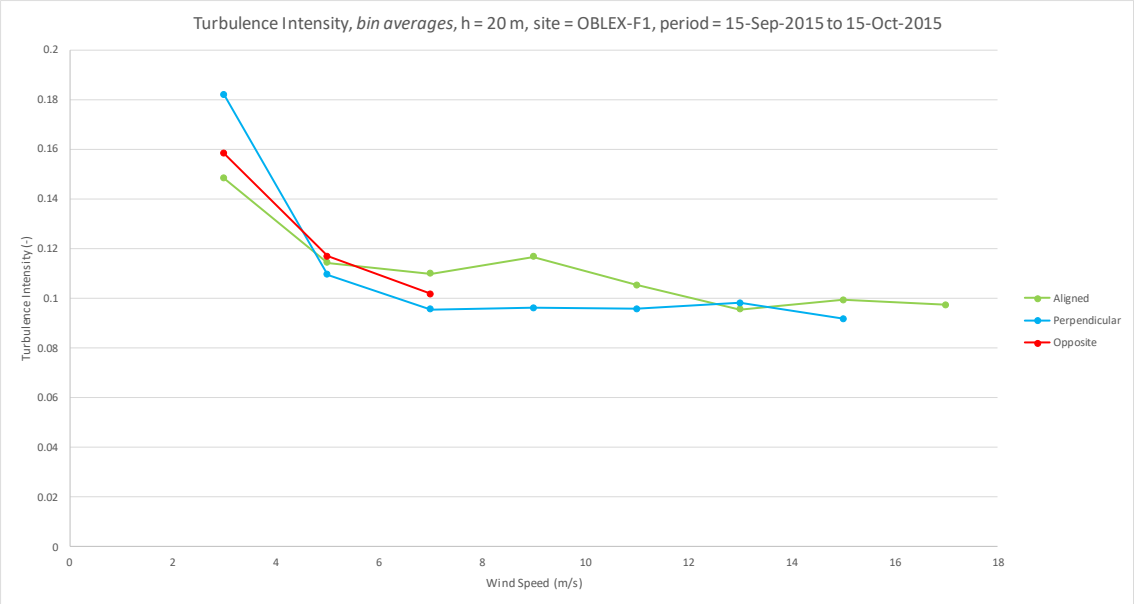

Figure 5.37 OBLEX-F1 Turbulence intensity bin averages at 20 m height for 1-month period.

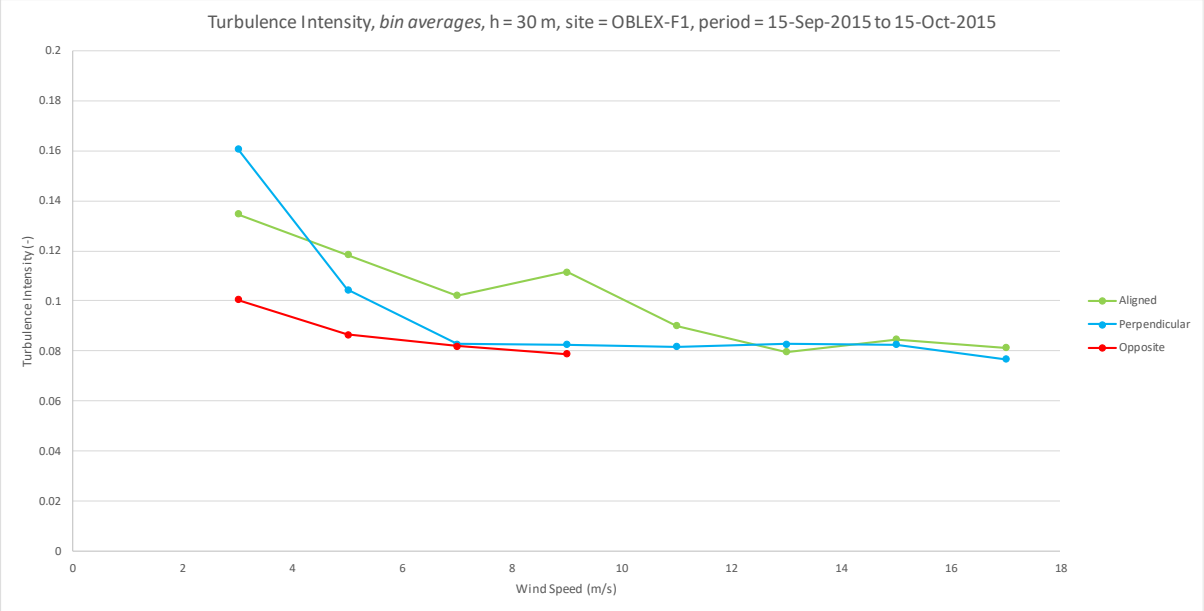

Figure 5.38 OBLEX-F1 Turbulence intensity bin averages at 30 m height for 1-month period.

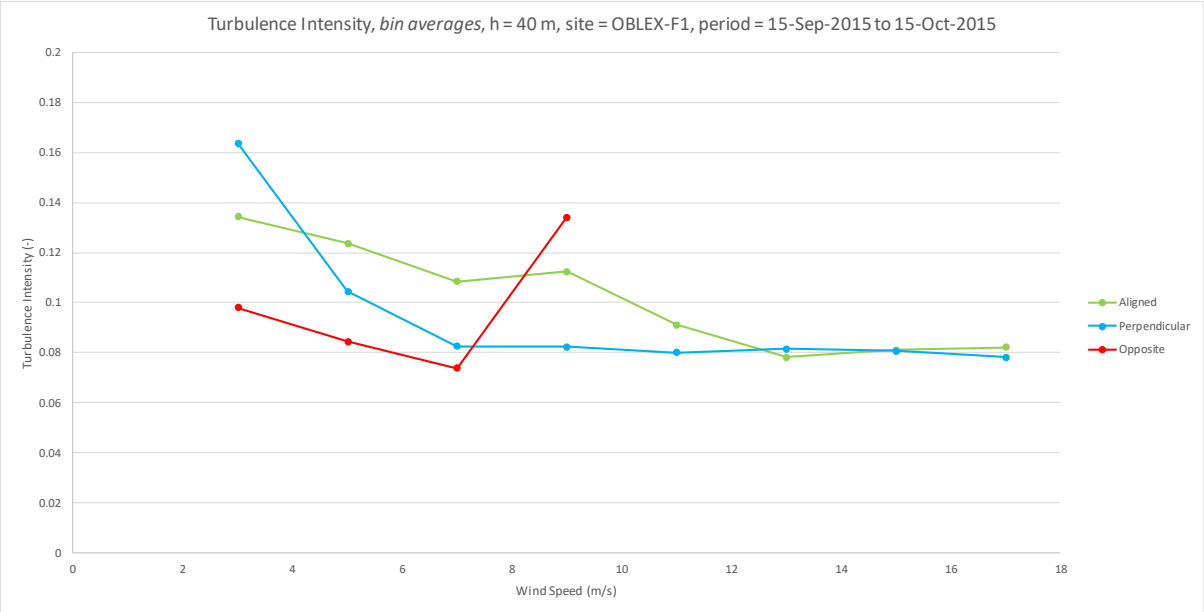

Figure 5.39 OBLEX-F1 Turbulence intensity bin averages at 40 m height for 1-month period.

There was similar pattern of the turbulence intensity plot for each misalignment condition at the four different heights, but enhanced turbulence was not observed for the opposite misalignment. It is plausible that the 1-month period data which were used to plot the wind speeds against turbulence intensities in these lower heights may not be enough to draw a firm conclusion to confirm this theory. Therefore, future research to include more data and longer than 1-month period may be necessary to be able to plot a wider range of turbulence intensities.

5.6 Offshore wind profile at FINO 1

Average wind profile at FINO 1 consist of FINO 1 data from 30 m to 100 m and OBLEX data at 15 m and 20 m. The wind profiles were observed to resemble the logarithmic wind profile and the future forecast of wind speed at certain heights might well be estimated by this law. However, an extensive assessment on comparing the long-term measurement FINO 1 data to determine the models of wind profile at can be performed to get a clear estimation of wind speeds at different heights. As shown in Figure 5.40, wind profiles classified according to the misalignment conditions show that the wind profiles for the aligned, perpendicular, and opposing conditions were observed to have the similar pattern. An interesting feature has been found by observing the wind speed gaps on the wind profile plot. The wind speeds gap between the total wind profile to the perpendicular condition and the gap between the total wind profile to the opposing condition were showing a regular pattern.

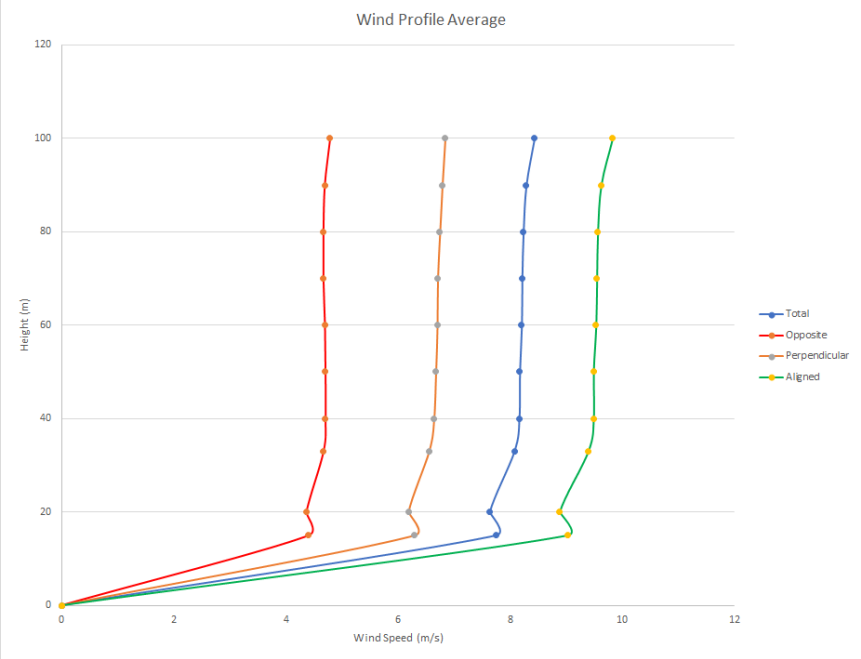

Figure 5.40 OBLEX-F1 mean wind profile classified by misalignment conditions.

Another interesting part from the mean wind profiles were the slightly higher mean wind speed at 15 m compared to the mean wind speed at 20 m. This may well be the fact that at sea, the lower boundary layer is not stationary due to wave, there could be an influence of shear stress on the surface of the sea that reinforcing the wind speed at near surface. Another reason of this phenomenon could be that there is an acceleration of wind speed because of the positioning of the sonic anemometers for both the lower heights measurement. The sonic anemometer at 15 m was mounted approximately 5.5 m from the railing of the round walk, whereas the sonic at

20 m was mounted approximately 4.5 m from the railing of the main platform deck. Moreover, there is 2 m difference in the width of the round walk and the platform deck. Therefore, there is 1 m gap in horizontal position between the two sonic anemometers that could result in a speed-up of the wind speed coming to the lowest 15 m sonic anemometers.

6. Conclusion

In this thesis, the occurrence of wind wave misalignment using 11 and 8 years of wind and wave data from the FINO 1 and FINO 3 measurement platforms was studied. The main conclusions are the following:

Total misalignment for each platform was, 36% for FINO 1 and 25% for FINO 3 while the opposing misalignment was 13% for FINO 1 and 9% for FINO 3. The condition of wind opposing swell waves has been identified in previous studies to have a significant impact the loading of offshore wind turbines (Kalvig, 2014; Sullivan et al., 2008) but our observations show that this is a relatively infrequent condition. Wind-wave misalignment under swell occurred less than the one under wind wave conditions with 14% misalignment under swell at FINO 1 and 17% at FINO 3. The condition of wind perpendicular to waves was more frequently observed with 23% occurrence at FINO 1 and 16% at FINO 3. Previous study by (Bachynski et al., 2014; Kalvig, 2014) have shown that wind-wave misalignment can have a significant impact on the motions and fatigue loads of fixed and floating offshore wind turbines. The results from this study suggest that the impact of wind perpendicular to waves on the loads and motions of offshore wind turbines should be further studied.

The turbulence intensities under different misalignment conditions and varying mean wind speeds was also investigated. The measurements showed that under opposing wind wave misalignment lower turbulence intensities were observed contrary to what was expected. Previous studies based on Large Eddy Simulations (LES) have shown enhanced turbulence intensities when the wind is opposing the waves especially under swell conditions. The mean peak period (Tp) for opposing misalignment was 8.7 s and 9.7 s at FINO 1 and FINO 3 respectively. The mean significant wave height (Hs) was 1.1 m and 0.89 m at FINO 1 and FINO 3 respectively for opposing misalignment. Therefore, a near swell wave system was expected to occur by the higher Tp and lower Hs. The wind speed vs wave height and wind speed vs wave period were plotted. The wave heights were not shown to have explain a higher surface roughness. Wave height and period give an indication of the surface roughness and therefore turbulence intensity. Previous studies have shown that under unstable conditions, there are higher turbulence intensities relative to stable conditions due to enhanced vertical mixing (Kalvig, Manger, et al., 2014). However, atmospheric stability also has a significant impact on turbulence intensities. Atmospheric stability was not considered in this study but should be considered in future work.

7. Future Work

An intensive analysis on the impact of atmospheric stability on turbulence intensity need to be carried in order to reach a conclusive reasoning behind the lower turbulence intensities found at opposing misalignment. More sets of data can be included for the OBLEX-F1 analysis further than 1-month duration, to get the wider range of turbulence intensity. Mean wind profile from FINO 1 and OBLEX data to be observed on a different time frame and a longer period data set. The long-term data sets for FINO 1 and FINO 3 with 11 years and 8 years respectively were sufficient to produce a reliable result for the frequency of occurrence of wind-wave misalignment. However, a methodology to interpolate the wave directions to match with the wind speeds data point can be done for future work, to get a more precise wave directionality.

References

Ackerman, D. S. (1995). Sea and Land Breezes. In.

Ainsworth, T. (2006). When Do Ocean Waves Become 'Significant'? A Closer Look at Wave Forecasts. *Mariners Weather Log, 50*(1).

Ameya, S., Sven-Erik, G., & Alfredo, P. (2011). Comparison of the atmospheric stability and wind profiles at two wind farm sites over a long marine fetch in the North Sea. *Wind Energy, 14*(6), 767-780. doi:doi:10.1002/we.456

Arya, S. P. (1988). Chapter 13 Marine Atmospheric Boundary Layer. In S. P. Arya (Ed.), *International Geophysics* (Vol. 42, pp. 197-222): Academic Press.

Babanin, A. V., & Soloviev, Y. P. (1998). Field Investigation of Transformation of the Wind Wave Frequency Spectrum with Fetch and the Stage of Development. *Journal of Physical Oceanography, 28*(4), 563-576. doi:10.1175/1520-0485(1998)028<0563:fiotot>2.0.co;2

Bachynski, E. E., Kvittem, M. I., Luan, C., & Moan, T. (2014). Wind-Wave Misalignment Effects on Floating Wind Turbines: Motions and Tower Load Effects. *Journal of Offshore Mechanics and Arctic Engineering, 136*(4), 041902-041902-041912. doi:10.1115/1.4028028

Badulin, S. I., Babanin, A. V., Zakharov, V. E., & Resio, D. (2007). Weakly turbulent laws of wind-wave growth. *Journal of Fluid Mechanics, 591*, 339-378. doi:10.1017/S0022112007008282

Barj, L., Jonkman, J. M., Robertson, A., Stewart, G. M., Lackner, M. A., Haid, L., . . . Stewart, S. W. (2014). Wind/Wave Misalignment in the Loads Analysis of a Floating Offshore Wind Turbine. In *32nd ASME Wind Energy Symposium*: American Institute of Aeronautics and Astronautics.

Barthelmie, R. J. (1999). Monitoring offshore wind and turbulence characteristics in Denmark.

Bartsch, C. (2015). Fact-Sheet Alpha Ventus. In.

Beeken, A., & Kindler, D. (2011). *Technical and Environmental Research Platforms for the Benefit of the Offshore Industry.* Paper presented at the BALTEXPO, Gdansk.

Bruno, P. (2017). What Is Wind Fetch?

Bundesamt für Seeschifffahrt und Hydrographie. (2018). FINO database. Retrieved from http://www.bsh.de/

Burton, T., Jenkins, N., Sharpe, D., & Bossanyi, E. (2001). *Wind Energy Handbook* (2nd ed.): Wiley.

Charnock, H. (1955). Wind stress on a water surface. *Quarterly Journal of the Royal Meteorological Society, 81*(350), 639-640. doi:10.1002/qj.49708135027

Cook, N. J. (1986). *Designers guide to wind loading of building structures. Part 1*.

Cushman-Roisin, B. (2014). *Environmental Fluid Mechanics*.

DNV-RP-C205. (2010). Environmental Conditions and Environmental Loads.

Emeis, S. (2012). *Wind Energy Meteorology: Atmospheric Physics for Wind Power Generation*: Springer Berlin Heidelberg.

Emeis, S. (2014). Current issues in wind energy meteorology. *Meteorological Applications, 21*(4), 803-819. doi:doi:10.1002/met.1472

Ernst, B., & Seume, J. R. (2012). Investigation of Site-Specific Wind Field Parameters and Their Effect on Loads of Offshore Wind Turbines. *Energies, 5*(10), 3835.

EWEA. (2009). *The Economics of Wind Energy* (S. Krohn Ed.).

Fischer, T., Rainey, P., Bossanyi, E., & Kühn, M. (2011). *Study on Control Concepts suitable for Mitigation of Loads from Misaligned Wind and Waves on Offshore Wind Turbines supported on Monopiles* (Vol. 35).

Flügge, M. (2018). NORCOWE OBLEX-F1 Campaign. In.

Flügge, M., & Løvset, T. (2018). NORCOWE OBLEX-F1 WEB PORTAL. http://www4.cmr.no:5000/help.html

Fontaine, E. (2013). A Theoretical Explanation of the Fetch- and Duration-Limited Laws. *Journal of Physical Oceanography, 43*(2), 233-247. doi:10.1175/jpo-d-11-0190.1

Foreman, R. J., & Emeis, S. (2010). Revisiting the Definition of the Drag Coefficient in the Marine Atmospheric Boundary Layer. *Journal of Physical Oceanography, 40*(10), 2325-2332. doi:10.1175/2010jpo4420.1

Freris, L. L. (1990). *Wind energy conversion systems*: Prentice Hall.

Gill Instruments Limited. (2013). R3-100 Datasheet. Retrieved from http://gillinstruments.com/products/anemometer/R3-100.html

Gosden, E. (2017). Record-breaking Hornsea Two wind farm will cut cost of green energy. Retrieved from https://www.thetimes.co.uk/article/record-breaking-wind-farm-will-cut-cost-of-green-energy-dong-energy-renewable-uk-hinkley-point-xfs0j893k

Gryning, S.-E., Batchvarova, E., Brümmer, B., Jørgensen, H., & Larsen, S. (2007). *On the extension of the wind profile over homogeneous terrain beyond the surface layer* (Vol. 124).

Hanley, K. E., Belcher, S. E., & Sullivan, P. P. (2010). A Global Climatology of Wind–Wave Interaction. *Journal of Physical Oceanography, 40*(6), 1263-1282. doi:10.1175/2010jpo4377.1

Hassan, G. (2018). The Atmospheric Boundary Layer Shear Profile. Retrieved from http://www.wind-energy-the-facts.org/best-practice-for-accurate-wind-speed-measurements-6.html

Hwang, P. A., & Wang, D. W. (2004). Field Measurements of Duration-Limited Growth of Wind-Generated Ocean Surface Waves at Young Stage of Development. *Journal of Physical Oceanography, 34*(10), 2316-2326. doi:10.1175/1520-0485(2004)034<2316:fmodgo>2.0.co;2

Janssen, P. (2004). *The Interaction of Ocean Waves and Wind*: Cambridge University Press.

Jenkins, M. (2005). Retrieved from http://ocw.usu.edu/Forest__Range__and_Wildlife_Sciences/Wildland_Fire_Management_and_Planning/Unit_7__Atmospheric_Stability_and_Instability_1.html

Kalvig, S. (2014). On wave-wind interactions and implications for offshore wind turbines. doi:10.13140/RG.2.1.2062.0322

Kalvig, S., Gudmestad, O. T., & Winther, N. (2014). Exploring the gap between 'best knowledge' and 'best practice' in boundary layer meteorology for offshore wind energy. *Wind Energy, 17*(1), 161-171. doi:10.1002/we.1572

Kalvig, S., Manger, E., Hjertager, B. H., & Jakobsen, J. B. (2014). Wave Influenced Wind and the Effect on Offshore Wind Turbine Performance. *Energy Procedia, 53*, 202-213. doi:https://doi.org/10.1016/j.egypro.2014.07.229

Kettle, A. J. (2013). FINO 1 - Research Platform in the North Sea.

Kühn, M. (2001). *Dynamics and design optimisation of offshore wind energy conversion systems*.

Martin, L. (2010). *Wind Energy – The Facts: A Guide to the Technology, Economics and Future of Wind Power* (Vol. 18).

Meteorologie. (2017). Retrieved from http://www.fino3.de/forschung/meteorologie

Motta, M., Barthelmie, R. J., & Vølund, P. (2005). The influence of non-logarithmic wind speed profiles on potential power output at Danish offshore sites. *Wind Energy, 8*(2), 219-236. doi:doi:10.1002/we.146

Neumann, T. (2007). FINO1 and The Mast Shadow Effect.

NORCOWE. (2018). *Norcowe OBLEX-F1 Data Extraction Portal*.

Obhrai, C., Kalvig, S., & Gudmestad, O. (2012). *A review of current guidelines and research on wind modeling for the design of offshore wind turbines*.

Peterson, E. W., & Jr., J. P. H. (1978). On the Use of Power Laws for Estimates of Wind Power Potential. *Journal of Applied Meteorology, 17*(3), 390-394. doi:10.1175/1520-0450(1978)017<0390:otuopl>2.0.co;2

Pettersson, H., Kahma, K., & Tuomi, L. (2010). *Wave Directions in a Narrow Bay* (Vol. 40).

Putri, R. M. (2016). *A Study of the Coherences of Turbulent Wind on a Floating Offshore Wind Turbine.* University of Stavanger, Norway.

Roy, S. B., & Sharp, J. (2013). Why Atmospheric Stability Matters in Wind Assessment. Retrieved from https://nawindpower.com/online/issues/NAW1301/FEAT_06_Why_Atmospheric.html

Semedo, A., Sušelj, K., Rutgersson, A., & Sterl, A. (2011). A Global View on the Wind Sea and Swell Climate and Variability from ERA-40. *Journal of Climate, 24*(5), 1461-1479. doi:10.1175/2010jcli3718.1

Simm, J., Brampton, A. H., Beech, N. W., Research, C. I., Association, I., & Brooke, J. S. (1996). *Beach Management Manual*: Construction Industry Research and Information Association.

Stiassnie, M. (2012). Fetch-limited growth of wind waves. *Journal of Geophysical Research: Oceans, 117*(C11). doi:doi:10.1029/2011JC007579

Stull, R. B. (1988). *An Introduction to Boundary Layer Meteorology*: Kluwer Academic Publishers.

Stull, R. B. (2000). *Meteorology for Scientists and Engineers*.

Sullivan, P. P., Edson, J. B., Hristov, T., & McWilliams, J. C. (2008). Large-Eddy Simulations and Observations of Atmospheric Marine Boundary Layers above Nonequilibrium Surface Waves. *Journal of the Atmospheric Sciences, 65*(4), 1225-1245. doi:10.1175/2007jas2427.1

Svardal, B. (2015). *The FINO1 measurement campaign, OBLEX-F1*. Retrieved from http://www.norcowe.no/doc//Annual%20Reports/Annual%20report%20NORCOWE%202015.pdf

Thompson, N. (1979). Boundary layer climates. By T. R. Oke. Methuen Ltd. 1978. *Quarterly Journal of the Royal Meteorological Society, 105*(446), 1084-1085. doi:doi:10.1002/qj.49710544628

Toba, Y. (1973). Local balance in the air-sea boundary processes. *Journal of the Oceanographical Society of Japan, 29*(5), 209-220. doi:10.1007/BF02108528

Twin Groves: A Lesson in Wind. (2016). Retrieved from https://www.geocaching.com/geocache/GC1BF99_twin-groves-a-lesson-in-wind?guid=04d4478a-f225-4de9-9c33-680dbcdd70aa

Vledder, G. (2013). On Wind-Wave Misalignment, Directional Spreading and Wave Loads. *5*. doi:10.1115/OMAE2013-11393

Westerhellweg, A., Canadillas, B., & Neumann, T. (2010). Direction Dependency of Offshore Turbulence Intensity in The German Bight.

Westerhellweg, A., Neumann, T., & Riedel, V. (2012). FINO1 Mast Correction. *DEWI Magazin*.

Wieringa, J. (1973). *Gust factors over open water and built-up country* (Vol. 3).

Windspeed Limited. (2018). A100 Series Anemometer. Retrieved from http://www.windspeed.co.uk/ws/index.php?option=displaypage&op=page&Itemid=48

Young, I. R. (1999). *Wind generated ocean waves / Ian R. Young*. Amsterdam ; Oxford: Elsevier.